Autoregulation clamps the synaptic membrane-remodeling machinery and promotes productive actin-dependent endocytosis

Steven J. Del Signore[a], Charlotte F. Kelley[a], Emily M. Messelaar[a], Tania Lemos[a], Michelle F. Marchan[a], Biljana Ermanoska[a], Markus Mund[b], Marko Kaksonen[b], Avital A Rodal[a1]

[a] Department of Biology, Brandeis University, 415 South St. Waltham MA USA

[b] Department of Biochemistry and NCCR Chemical Biology, University of Geneva, 30 Quai Ernest-Ansermet, 1211 Geneva, Switzerland

[1] Correspondence: arodal@brandeis.edu, Brandeis University 415 South St MS029 Waltham MA 02454 781-736-2459

Abstract

Synaptic membrane-remodeling events such as endocytosis require force-generating actin assembly. The endocytic machinery that regulates these actin and membrane dynamics localizes at high concentrations in a micron-scale synaptic membrane domain called the 'periactive zone' (PAZ). Paradoxically, endocytic events occur only sparsely in space and time within the PAZ. Here we describe a mechanism whereby autoinhibition clamps the PAZ machinery to limit actin assembly to discrete functional events. We found that collective interactions between the *Drosophila* PAZ proteins Nwk/FCHSD2, Dap160/Intersectin, and WASp relieve Nwk autoinhibition and promote robust membrane-coupled actin assembly *in vitro.* Using automated particle tracking to quantify synaptic actin dynamics *in vivo*, we discovered that Nwk-Dap160 interactions constrain spurious assembly of WASp-dependent actin structures. These interactions also promote synaptic endocytosis, suggesting that autoinhibition both clamps and primes the synaptic endocytic machinery, thereby constraining actin assembly to drive productive membrane remodeling in response to physiological cues.

Keywords: Endocytosis, actin, cytoskeleton, membrane remodeling, synapse, WASp, Intersectin, Nervous Wreck, traffic, autoinhibition

Introduction

In diverse types of neurons, sites of synaptic vesicle release are surrounded by a micron-scale membrane domain called the periactive zone (PAZ, **Fig 1A**), in which the endocytic machinery cooperates with the actin cytoskeleton to drive synaptic vesicle membrane and protein recycling, internalization of signaling receptors, and synapse morphogenesis (Kaempf and Maritzen, 2017). Unlike non-neuronal cells, in which endocytic proteins are transiently recruited from the cytosol to active sites of actin-dependent membrane internalization (Kaksonen and Roux, 2018), presynaptic terminals maintain a constitutively high local concentration of endocytic proteins, either associated with the synaptic vesicle pool (Denker et al., 2011; Winther et al., 2013, 2015) or in the PAZ as a 'readily retrievable pool' (Hua et al., 2011; Wilhelm et al., 2014). As only a small fraction of this endocytic protein pool is likely to be engaged in endocytosis at any point in time (in response to vesicle release) and space (at <100 nm diameter endocytic sites within the PAZ), synapses have the unique property that the endocytic apparatus must be held in a primed, yet inactive state at the membrane. This clamping/priming provides one potential mechanism to ensure that individual synapses are poised for rapid recycling of membranes and proteins when necessary (Pelassa et al., 2014). However, the mechanisms that allow for accumulation of the endocytic machinery at the membrane while maintaining them in an inactive state are not known.

One plausible mechanism to restrict membrane-cytoskeleton remodeling and endocytic activity in space and time may lie in the autoinhibition of PAZ proteins. One example is the F-BAR-SH3 protein Nervous Wreck (Nwk), which regulates synaptic membrane traffic at the *Drosophila* neuromuscular junction (NMJ) (Coyle et al., 2004; O'Connor-Giles et al., 2008; Rodal et al., 2008, 2011; Ukken et al., 2016) and whose mammalian homolog FCHSD2 regulates endocytosis in mammalian cells (Almeida-Souza et al., 2018; Xiao et al., 2018). Nwk and FCHSD2 couple two activities: membrane remodeling and WASp-dependent actin polymerization, both of which are subject to autoregulation (Almeida-Souza et al., 2018; Rodal et al., 2008; Stanishneva-Konovalova et al., 2016). Specifically, interactions between the Nwk F-BAR and SH3 domains mutually inhibit Nwk membrane binding and activation of WASp (Stanishneva-Konovalova et al., 2016). Unlike other F-BAR-SH3 proteins, which are completely released from autoinhibition upon membrane binding (Guerrier et al., 2009; Meinecke et al., 2013; Rao et al., 2010), the SH3b domain of Nwk continues to restrict SH3a-mediated WASp activation even after Nwk binds membranes. This suggests that autoinhibition allows Nwk-WASp to remain inactive even after recruitment to the membrane, thus keeping the endocytic machinery in a primed but inactive state. We hypothesized that additional binding partners of Nwk^{SH3b} may be required to fully activate membrane remodeling at discrete times and locations in the PAZ (**Fig 1B**).

An excellent candidate for release of Nwk autoinhibition at synapses is the endocytic adapter Intersectin (Dap160 in *Drosophila*). Intersectin interacts with numerous endocytic proteins to regulate endocytosis in mammalian cells (Henne et al., 2010; Okamoto et al., 1999; Praefcke et al., 2004; Pucharcos et al., 2000; Schmid et al., 2006; Sengar et al., 1999; Teckchandani et al., 2012), and has been implicated in several steps of the synaptic vesicle cycle (Evergren et al., 2007; Gerth et al., 2017; Jäpel et al., 2020; Pechstein et al., 2010, 2015). Of particular note, Intersectin recruits the Nwk homolog FCHSD2 to sites of endocytosis (Almeida-Souza et al., 2018), though it is not yet known how this affects FCHSD2 autoinhibition. In *Drosophila*, Dap160 interacts with WASp, Nwk, and other PAZ proteins via its four SH3 domains (SH3A-D), and regulates the levels and localization of many of these proteins, including Nwk (Koh et al., 2004; Marie et al., 2004;

Roos and Kelly, 1998). Further, *dap160* mutant phenotypes overlap with those of Nwk and WASp mutants, including impaired synaptic vesicle cycling and synaptic overgrowth (Coyle et al., 2004; Khuong et al., 2010; Koh et al., 2004; Marie et al., 2004). Finally, Intersectin and Dap160 shift localization from synaptic vesicle pools to the PAZ in response to synaptic activity (Evergren et al., 2007; Gerth et al., 2017; Winther et al., 2015), suggesting that Dap160 may provide the spatiotemporal link between salient physiological triggers and Nwk/WASp activation.

Characterizing the activation of the synaptic endocytic apparatus *in vivo* is challenging, due to the difficulty of visualizing productive endocytic events among a large pool of inactive endocytic proteins. To overcome this challenge, we utilized actin assembly at the *Drosophila* NMJ as a proxy for productive endocytosis, as actin assembly is both a primary target of the endocytic apparatus under investigation, and is required for synaptic vesicle endocytosis in all forms, including at the *Drosophila* NMJ (Kononenko et al., 2014; Wang et al., 2010; Wu et al., 2016). This synapse is an ideal system to investigate the molecular dynamics of the endocytic machinery due to its large size, ease of genetic manipulation, and accessibility to live and super-resolution imaging. Here we combine *in vitro* biochemical approaches with quantitative imaging at the NMJ to define the interactions among Dap160, Nwk, and WASp that relieve autoinhibition. These interactions drive robust membrane-associated actin assembly *in vitro*, regulate the frequency and dynamics of synaptic actin structures *in vivo*, and are functionally required for normal endocytosis at the NMJ.

Results

Membrane-cytoskeleton remodeling proteins in the PAZ are distributed broadly but activated locally

Using conventional and super-resolution microscopy of neurons in diverse organisms, the presynaptic membrane remodeling machinery has been found to localize to a broad membrane domain surrounding active zones, termed the periactive zone (PAZ) (Coyle et al., 2004; Denker et al., 2011; Gerth et al., 2017; Koh et al., 2004; Marie et al., 2004; Sone et al., 2000). Consistent with these prior descriptions, we observed by structured illumination microscopy (SIM) that the PAZ proteins Nwk and Dap160 localize to a membrane proximal reticulum that surrounds the active zone protein Bruchpilot (BRP, **Fig 1A**). Similar results were observed for Nwk using live imaging of the endogenously tagged protein (**Fig S1A**).

To identify sites where the endocytic machinery is active, we analyzed the distribution and dynamics of F-actin. While the importance of actin in synaptic endocytosis is clear (Kononenko et al., 2014; Wang et al., 2010; Wu et al., 2016), until now there has been no quantitative analysis of individual actin-dependent membrane-remodeling events at synapses. To bridge this gap, we performed spinning disk confocal microscopy of NMJs presynaptically expressing a GFP-tagged F-actin binding domain (GMA). GMA predominantly appeared at the presynaptic membrane in transient, largely stationary patches (**Movie 1, Fig S1A-B**), as has been previously observed (Nunes et al., 2006; Pawson et al., 2008; Piccioli and Littleton, 2014). We then quantified individual actin patch

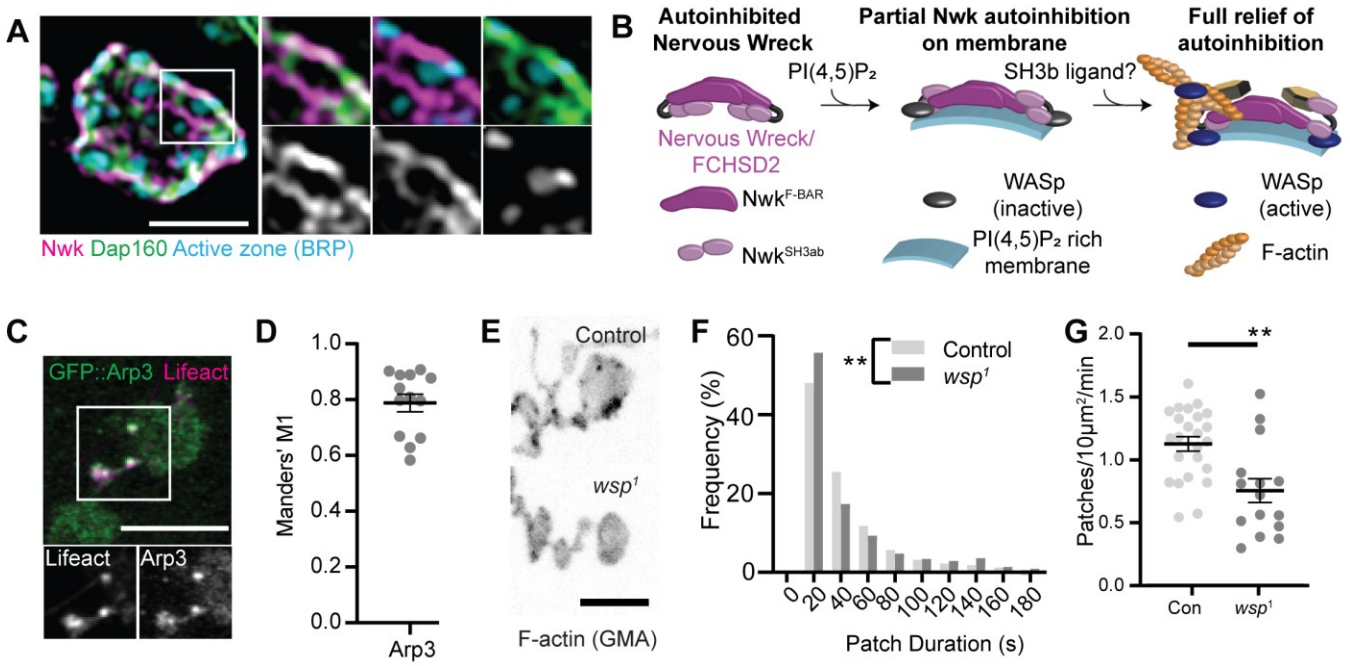

Figure 1. Periactive zone proteins exhibit broad localization but discrete activation. (A) The periactive zone (PAZ) proteins Nwk (magenta) and Dap160 (green) accumulates in a micron-scale reticulum adjacent to active zones (AZ) (Bruchpilot, blue). Image shows maximum intensity projection (MaxIP) of a structured illumination microscopy (SIM) Z-stack. (B) Model for autoinhibition of Nwk membrane binding and WASp activation. Neither membrane-bound or membrane-free Nwk efficiently activate WASp-mediated actin polymerization, due to persistent SH3b-mediated autoinhibitory interactions, suggesting that an SH3b domain ligand is required for activation. (C) MaxIPs (Airyscan microscopy) of a single frame of muscle 6/7 NMJ expressing Lifeact::ruby (magenta, left inset) Arp3::GFP (green, right inset). Actin patches colocalize extensively with Arp3::GFP. (D) Quantification of colocalization by Manders' coefficients. Graph shows mean +/- s.e.m.; n represents NMJs. (E-G) Patch assembly requires the Arp2/3 activator WASp. MaxIPs of single spinning disk confocal microscopy time points, showing pan-neuronally expressed GMA localization in control and *wsp*[1] mutant m6/7 NMJs. (F) Quantification of patch duration distribution. Bins are 20 sec; X axis values represent bin centers. n represents patches. (G) Quantification of patch frequency. Graph shows mean +/- s.e.m.; n represents NMJs. Scale bars in A, C, E are 2.5 µm. Associated with Fig. S1 and Movie 1.

dynamics using automated particle tracking and quantification (Berro and Pollard, 2014), which captured on the order of 30-50% of visible actin structures (based on the number of candidates rejected during track curation). Imaging at .25Hz, we found an average of 1.2 GMA patches/10μm^2/min, exhibiting a mean duration of 48.0 sec +/- 45.6 sec, with an average relative amplitude of 68%+/- 32% ((I_{max}-I_{min})/I_{mean}) (**Fig S1C-F**). As we noted a strong floor effect with short-duration patches, we also performed imaging at 1Hz, which identified a higher frequency of shorter duration patches (**Fig S1G**). Given these measurements and the efficiency of our automated detection, we estimate that patch frequency is approximately ~4-6 events/10 μm^2/min. We found similar properties for another F-actin binding peptide, Lifeact::Ruby, as well as for GFP labeled actin itself (**Fig S1C-F**).

We next examined the molecular determinants of synaptic actin patch assembly. Patches strongly co-labeled with Arp3::GFP (Manders' coefficient of .81 (Lifeact:Arp3), (**Fig 1C-D**)), suggesting they are

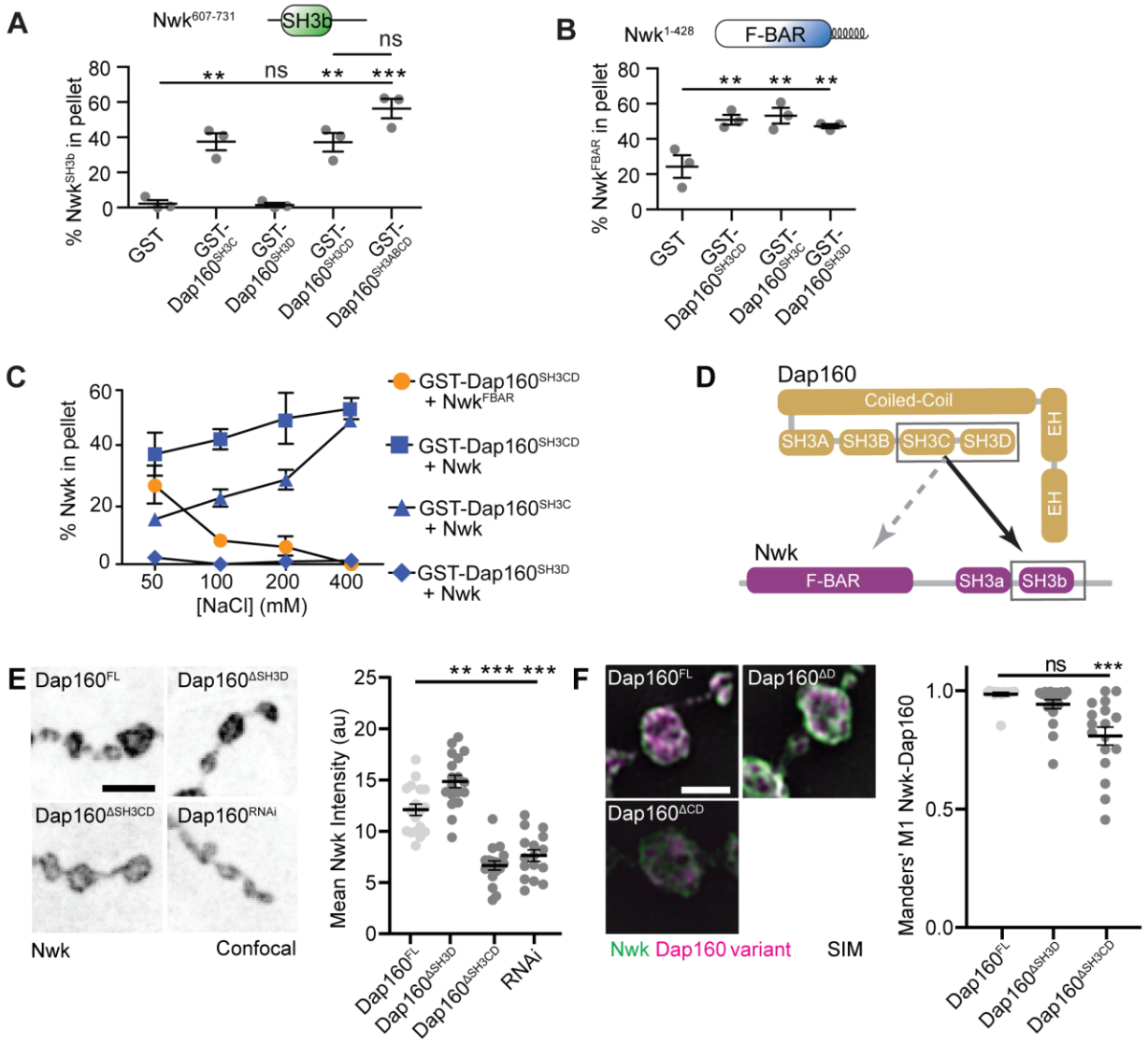

Figure 2. Distinct SH3-SH3 and SH3-BAR domain interactions drive Dap160-Nwk association *in vitro* and at synapses. (A-C) GST fusion proteins were immobilized on glutathione agarose and incubated with the indicated purified proteins. Pellets and supernatants were fractionated by SDS-PAGE, immunoblotted (A) or Coomassie stained (B-C), and quantified by densitometry. Graphs show the average +/- s.e.m. of three independent reactions. (A) Nwk^{SH3b} interacts directly with Dap160^{SH3C}, Dap160^{SH3CD} or Dap160^{SH3ABCD}, but not with Dap160^{SH3D} alone. [Nwk^{SH3b}]=7μM. (B) The Nwk F-BAR domain interacts directly with Dap160^{SH3}, Dap160^{SH3D}, and Dap160^{SH3CD}. [Nwk^{F-BAR}]=1.5μM, [GST-Dap160^{SH3CD}]=8.5μM, [GST-Dap160$^{SH3C/D}$]=11μM. (C) The Dap160^{SH3CD}-Nwk^{F-BAR} interaction is salt-sensitive, while the Dap160 interactions with Nwk SH3 domains are not. [Nwk^{F-BAR}]=1.5 μM, [Nwk]=.8μM, [GST-Dap160^{SH3CD}]=1.6μM, [GST-Dap160$^{SH3C/D}$]=1.2μM. (D) Summary of Dap160^{SH3CD}-Nwk^{SH3ab} interactions. Gray and black arrows indicate electrostatic and hydrophobic interactions, respectively (E) MaxIP spinning disc confocal or (F) MaxIP SIM micrographs of muscle 4 NMJs expressing C155-GAL4-driven UAS-Dap160 rescue transgene variants in a *dap160* null background (dap160$^{Δ1/Df}$). Loss of the Dap160^{SH3CD} domains (Dap160^{ΔSH3CD}), but not the SH3D domain alone (Dap160^{ΔSH3D}), disrupts normal Nwk accumulation (E, right) and Dap160-Nwk colocalization (F, right) at synapses. Graphs show mean +/- s.e.m.; n represents NMJs. Associated with **Fig S2**.

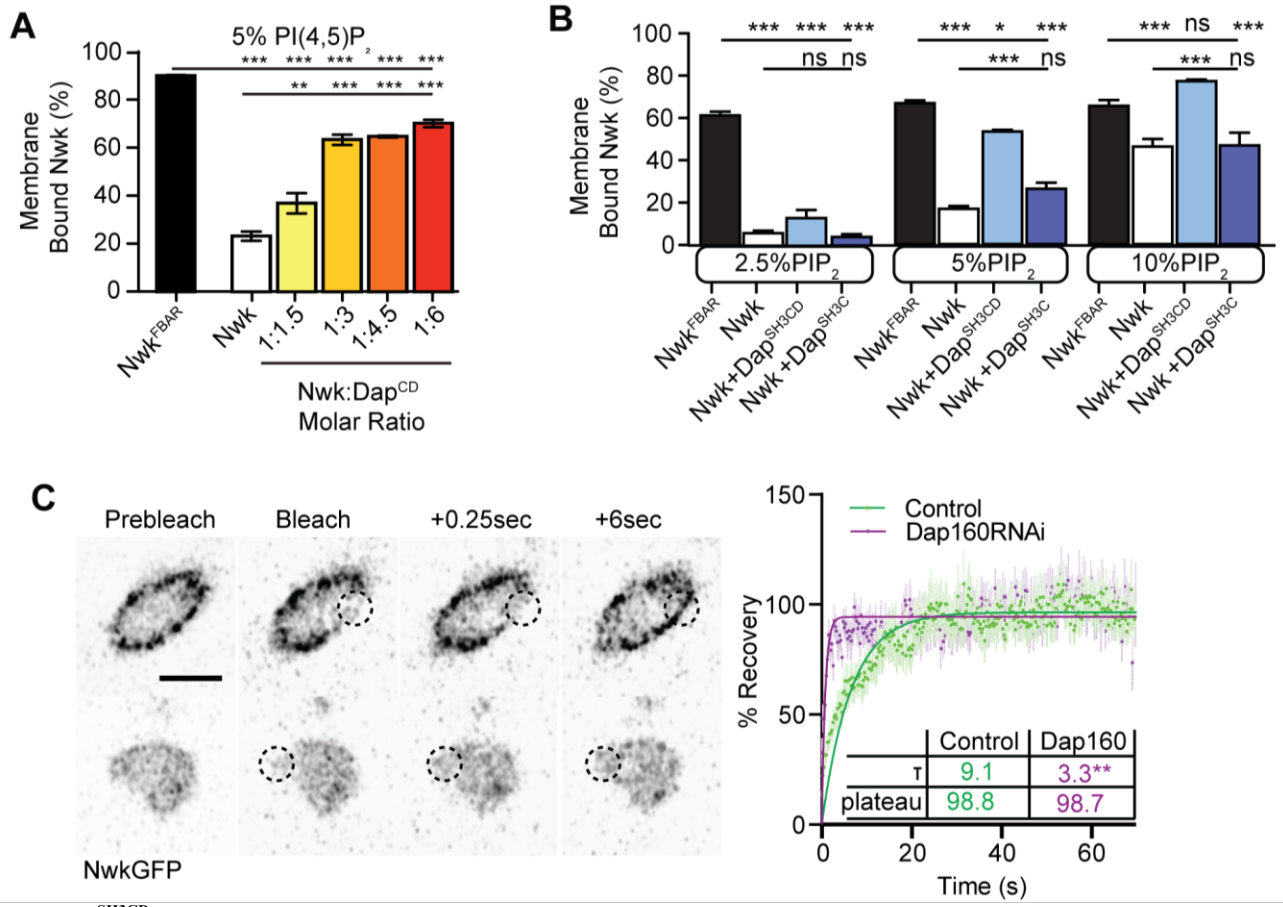

Figure 3. Dap160^{SH3CD} promotes Nwk membrane association. (A-B) Liposome co-sedimentation assays between the indicated purified proteins and liposomes composed of [mol% = DOPC/DOPE/DOPS/PI(4,5)P_2 = 80-x/15/5/x], with x representing PI(4,5)P_2 concentration as noted. Quantification from Coomassie-stained gels represents the mean fraction of total protein that cosedimented with the liposome pellet, ± SEM. (A) 1:3 Nwk:Dap160^{SH3CD} saturates enhancement of Nwk membrane association at 5% PI(4,5)P_2, but not to the level of the isolated Nwk F-BAR alone (Nwk$^{F\text{-}BAR}$, black bar). [Nwk$^{1\text{-}xxx}$] = 2µM, [Dap160] = 6µM. (B) Dap160^{SH3CD} (but not Dap160^{SH3C}) enhances Nwk association with membranes at a range of PI(4,5)P_2 concentrations. Maximum binding (comparable to Nwk$^{F\text{-}BAR}$ occurs only at 5-10% PI(4,5)P_2 concentrations. [Nwk$^{F\text{-}BAR}$] = 3µM, [Nwk] = 1.125µM, [Dap160^{SH3CD}] = 1.7-6.8µM. (C) FRAP assay of endogenously labeled Nwk in control and C155-GAL4/UAS-Dicer driven Dap160^{RNAi} NMJs. Images show individual medial optical sections of Airyscan confocal images at the indicated time point. Control Nwk signal shows strong membrane association (see strong peripheral signal) and slower recovery kinetics, while loss of Dap160 eliminates the strong peripheral accumulation of Nwk^{GFP} and increases the recovery kinetics of NwkGFP in the bleached region (dashed circles). Graph shows mean +/- s.e.m. ; n represents NMJs. Scale bar is 5 µm. Associated with **Fig S3**.

predominantly composed of branched F-actin, similar to sites of endocytosis in other cell types (Akamatsu et al., 2020; Collins et al., 2011). To test whether synaptic actin patches require Arp2/3 activation, we analyzed patch dynamics in larvae lacking the Arp2/3 activator WASp. We compared a genomic mutant (**Fig 1E-G**, likely hypomorphic due to maternal contribution (Ben-Yaacov et al., 2001)) to presynaptic depletion in neurons expressing WASp RNAi (**Fig S1H-J**). Using both approaches allows us to distinguish neuron-autonomous from non-autonomous effects of WASP, which is abundant at postsynaptic NMJ membranes (Coyle et al., 2004). Both genomic and RNAi manipulations significantly reduced the number of actin patches, while genomic mutants also skewed the distribution of patch durations towards both shorter and longer events (**Fig 1F**). These differences could reflect variable loss of function between the RNAi and mutant, or identify separable presynaptic autonomous (patch frequency), vs non-autonomous (patch duration) effects of WASp. Overall, these data clearly indicate that WASp is autonomously required in neurons to initiate assembly of presynaptic actin patches, similar to its involvement in endocytosis in yeast, mammalian non-neuronal cells, and in the NMJ (Hussain et al., 2001; Kessels and Qualmann, 2004; Khuong et al., 2010; Madania et al., 1999).

Finally, we analyzed the localization of PAZ proteins relative to F-actin at the NMJ. GMA only partially overlapped with each of presynaptic WASp, Nwk, and Dap160 (**Fig S1K-M)**; Manders' coefficients of 0.45, 0.59, 0.53, respectively). Together, these data confirm that, in sharp contrast to the endocytic actin regulatory machinery, which localizes broadly across the PAZ, actin assembly itself is restricted both spatially and temporally at the NMJ. This raises the question of how PAZ machinery might itself be locally regulated to promote the formation of productive synaptic actin assemblies.

Multiple interaction interfaces between Dap160 and Nwk regulate Nwk autoinhibition

The hypothesis that PAZ protein-mediated actin assembly might be locally activated is particularly interesting given that we and others have previously shown that both Nwk and its mammalian homolog FCHSD2 can only weakly activate WASp, due to Nwk autoinhibition (Almeida-Souza et al., 2018; Rodal et al., 2008; Stanishneva-Konovalova et al., 2016). Thus, transient or localized relief of autoinhibition, perhaps by the Nwk-binding partner Dap160, could explain how the PAZ generates targeted actin dynamics. To determine if and how Dap160 might relieve Nwk autoinhibition, we first mapped their specific interaction domains and found that purified Dap160 SH3C containing protein fragments (SH3C, SH3CD, or SH3A-D) directly interact with Nwk^{SH3b}, while SH3D alone does not (**Fig 2A, Fig S2A,** see **Fig S2D** for details of constructs used). Unexpectedly, Dap160 SH3C, SH3D, and SH3CD domain fragments also each interact with the isolated Nwk F-BAR domain (**Fig 2B, Fig S2B**). We next determined how Dap160 interactions with Nwk$^{F\text{-}BAR}$ compared to a near-full length Nwk fragment containing the F-BAR and both SH3 domains, which is sufficient to rescue the *nwk* mutant phenotype (Rodal et al., 2008). Dap160-Nwk$^{F\text{-}BAR}$ interactions were progressively eliminated by increasing salt, suggesting they are mediated by electrostatic interations. By contrast, Dap160-Nwk interactions were maintained (**Fig 2C, Fig S2C**), suggesting this SH3-SH3 interface is mediated primarily by hydrophobic interactions, consistent with their mammalian homologs (Almeida-Souza et al., 2018) (see summary of interactions, **Fig 2D**). Consistent with a bona fide *in vivo* activity, truncation of Dap160^{SH3CD} significantly decreased the levels of Nwk in synaptic boutons (**Fig 2E, Fig S2D-F**) as well as colocalization between Nwk and Dap160 (**Fig 2F**).

Dap160 relieves Nwk autoinhibition and promotes its membrane association

To understand how Dap160 might regulate the molecular activity of

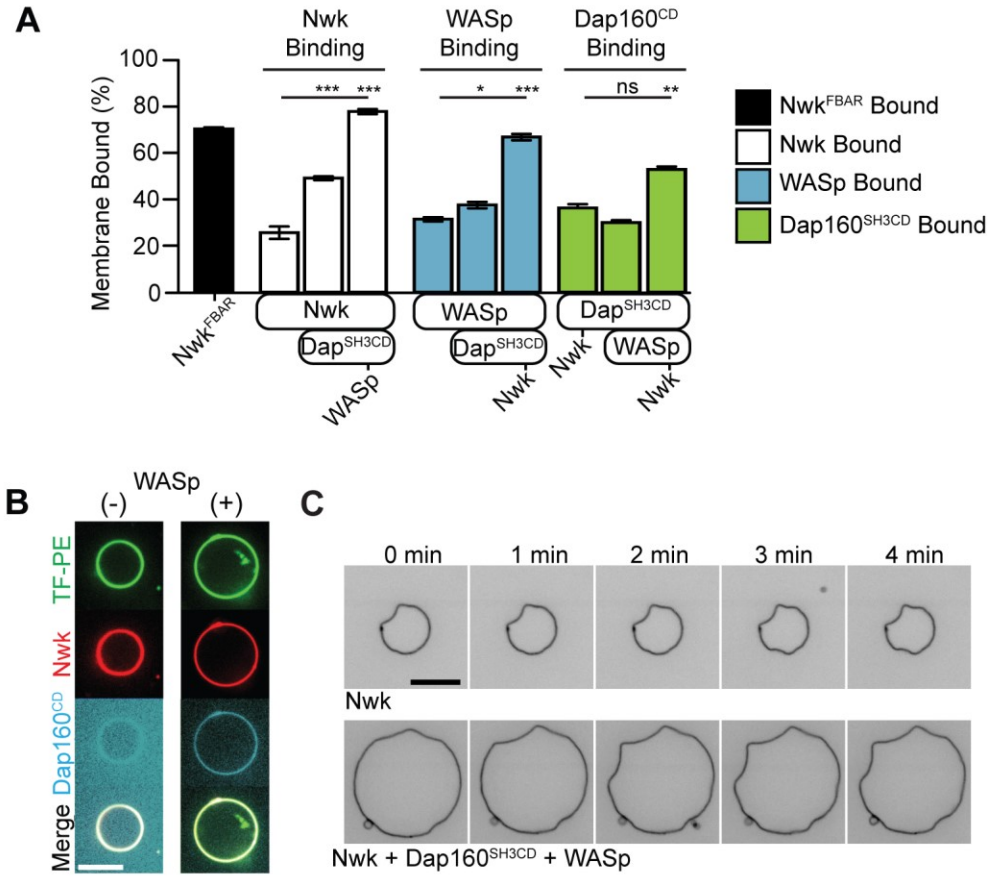

Figure 4. Dap160^{SH3CD} and WASp collaboratively promote Nwk membrane association. (A) Cosedimentation assay between the indicated purified proteins and liposomes composed of [mol% = DOPC/DOPE/DOPS/PI(4,5)P_2 = 70/15/5/10]. Nwk, WASp, and Dap160^{SH3CD} mutually enhance membrane recruitment. Addition of Dap160^{SH3CD} and WASp additively enhance Nwk membrane association, while Dap160^{SH3CD} and WASp show maximum recruitment to PI(4,5)P_2 liposomes in the presence of both other proteins. [Nwk] = 1µM, [WASp] = 1µM, [Dap160^{SH3CD}] = 3µM. (B) GUV decoration assay, with 10% PI(4,5)P_2 GUVs labeled with <1% TopFluor-PE. The addition of WASp to Nwk (red) and Dap160^{SH3CD} (blue) enhances the recruitment of Dap160^{SH3CD} to the membrane (green, note diffuse blue signal in (-) WASp condition). [Nwk] = 250nM, [WASp] = 250nM, [Dap160^{SH3CD}] = 1µM (C) Confocal timelapse of deformation of GUVs (10% PI(4,5)P_2, labeled with <1% TopFluor-PE) decorated with the indicated proteins [Nwk$^{1\text{-}xxx}$] = 250nM, [WASp]=250nM, [Dap160] = 1.25µM. The Nwk-Dap160-WASp complex retains the same membrane remodeling activity as Nwk alone. Scale bars in (B,C) are 10 µm. Associated with **Fig S4**.

Nwk, we first tested whether Dap160^{SH3CD} regulates Nwk membrane binding. We found that Dap160^{SH3CD} enhanced Nwk membrane binding in a dose-dependent fashion, saturating at stoichiometries of 1:3 (Nwk:Dap160) (**Fig 3A**). Because intramolecular Nwk SH3-F-BAR interactions mediate autoinhibition of both actin assembly and membrane binding (Stanishneva-Konovalova et al., 2016), we hypothesized that coordinated binding between Dap160^{SH3D}-Nwk^{F-BAR} and Dap160^{SH3C}-Nwk^{SH3b} might be required to activate Nwk. We first tested whether Dap160 relieves autoinhibition of Nwk membrane-binding, using liposome cosedimentation assays. We previously found that Nwk^{F-BAR} membrane association depends strongly on charged phosphoinositides (Becalska et al., 2013; Kelley et al., 2015) and that

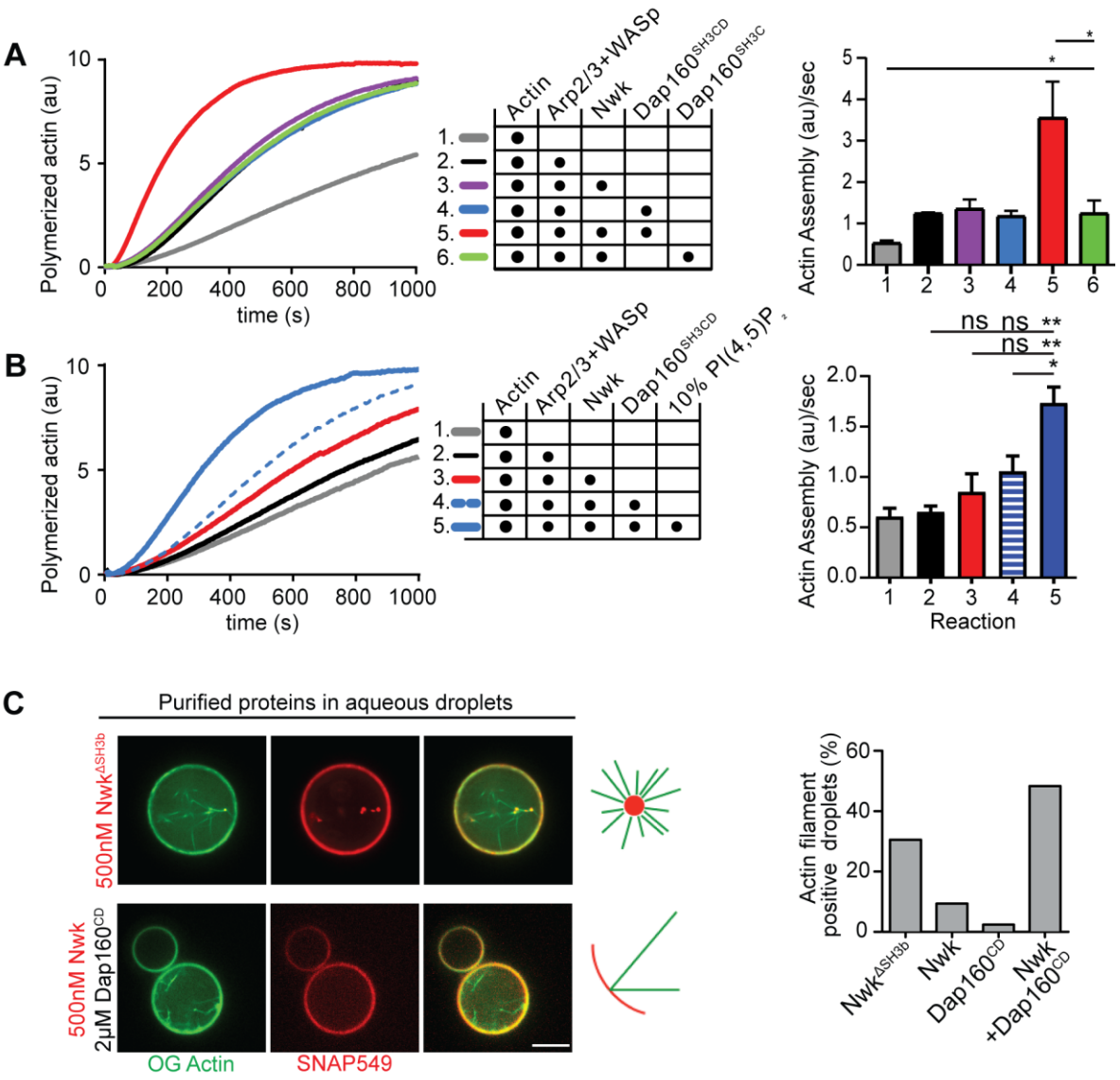

Figure 5. Nwk, Dap160, and PI(4,5)P$_2$ potentiate WASp-mediated actin assembly at membranes. (A-B) Pyrene actin assembly assay (2.5μM actin, 5% pyrene labeled). Curves are representative single experiments demonstrating actin assembly kinetics; graphs represent rates calculated from the linear range of assembly from at least two independent experiments. (A) The combination (red trace) of Nwk and Dap160^{SH3CD} together enhance WASp-Arp2/3 mediated actin assembly. Either alone (magenta and blue traces) has no effect on WASp activity. [Nwk] = 500nM, [Dap160] = 2μM, [WASp] = 50nM, [Arp2/3] = 50nM. (B) PI(4,5)P$_2$ enhances Nwk-Dap160 activation of WASp-mediated actin assemby. Nwk alone or in combination with 10% PI(4,5)P$_2$ liposomes fails to activate WASp, while the addition of Dap160^{SH3CD} and PI(4,5)P$_2$ synergistically enhance WASp-mediated actin assembly. [Nwk] = 100nM, [Dap160] = 500nM, [WASp] = 50nM, [Arp2/3] = 50nM. (C) Single slices from spinning disc confocal micrographs of water-droplet actin assembly assay: SNAP labeled Nwk constructs (red) and Oregon Green actin (green) were mixed with the indicated proteins in aqueous solution and emulsified in 97.5% DPHPC, 2.5% PI(4,5)P$_2$ in decane. Both deregulated Nwk$^{\Delta SH3b}$ and Nwk + Dap160^{SH3CD} promote F-actin assembly in droplets. However, while Nwk-DapCD derived F-actin associates with the lipid interface, de-regulated Nwk$^{\Delta SH3b}$ promotes actin assembly from asters that do not associate with membrane. [Nwk^{1-xxx}] = 500nM, [Dap160] = 2μM, [WASp] = 50nM, [Arp2/3] = 50nM.Graph indicates percentage of droplets with observable actin filament assembly. Scale bar in C is 10μm.

Nwk$^{1-731}$ (containing both autoinhibitory SH3 domains) requires higher phosphoinositide levels for membrane binding. At intermediate phosphoinositide concentrations, Dap160^{SH3CD} significantly enhanced membrane binding by Nwk (**Fig 3B**). However, Dap160^{SH3C} was unable to promote membrane binding by Nwk, indicating that the Da160^{SH3C}-Nwk^{SH3b} interaction is not sufficient for full relief from autoinhibition. As we found that loss of SH3D alone did not perturb Nwk distribution or function *in vivo* (**Fig 2E-F, Fig 7F-G**), it is likely that these additional interactions can be fulfilled by any of SH3A,B, or D, or perhaps by an alternative binding partner.

We then asked whether Dap160^{SH3CD}-mediated enhancement of Nwk membrane binding was indeed through relief of Nwk^{SH3b}. Dap160^{SH3CD} had no effect on membrane binding by Nwk lacking its Dap160-binding SH3b domain (Nwk$^{\Delta SH3b}$, **Fig S4A**). Finally, to test if Dap160 might promote Nwk membrane association *in vivo*, we examined the dynamics of Nwk at the synapse in the presence and absence of Dap160. Knockkdown of Dap160 by RNAi (**Fig 3C, Fig S3A**) led to a striking loss of endogenous Nwk^{GFP} from synaptic membranes (note strong peripheral labeling in control bouton cross-sections, **Fig 3C**). Further, Dap160 knockdown significantly increased the recovery kinetics of Nwk^{GFP}, consistent with a shift in localization from membrane-bound to cytosolic. These data indicate that the Dap160^{SH3CD}-Nwk interaction promotes not only Nwk abundance (**Fig 2E**) but also Nwk membrane association *in vivo*.

Dap160 and WASp cooperate to relieve autoinhibition of Nwk membrane binding and actin assembly

We noted that Dap160^{SH3CD} is insufficient to fully activate membrane binding by Nwk compared to the F-BAR domain alone at intermediate phosphoinositide concentrations (**Fig 3A**). This is consistent with our prior observation that truncation of SH3b only partially relieved Nwk autoinhibition, and suggests that ligands other than Dap160 (perhaps of

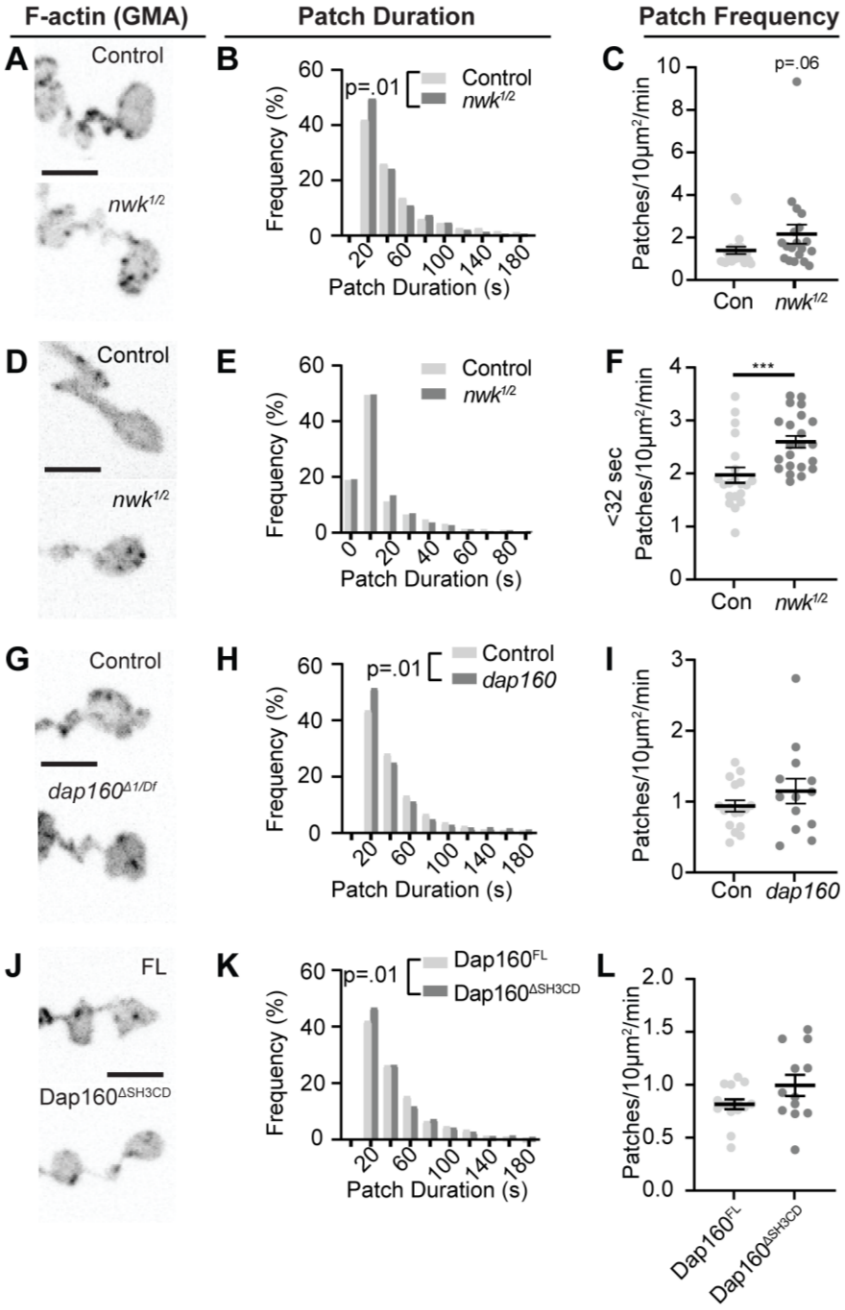

Figure 6. Loss of the Dap160-Nwk interaction disrupts actin patch dynamics at synapses *in vivo*. Quantification of GMA-labeled F-actin patch dynamics. All imaging was performed at .25Hz, except (D-F), which was performed at 1Hz. (A,D,G,J) maxIPs of live spinning disc confocal micrographs of GMA in the indicated genotypes. Graphs quantify distribution of patch durations (B,E,H,K) and patch frequency (C,F,I, L). Loss of each of *nwk* (A-C) alters the distribution of patch durations, with a greater fraction of short-lived (16-30 sec). (D-F) Imaging at 1 frame/sec confirms a significant increase in the frequency of short-lived (<32sec) patches. Loss of *dap160* (D-F), or the Nwk-interacting Dap160^{SH3CD} domain similarly alters the distribution of patch durations (p<.01, KS test), with a particular increase in the frequency of short-lived (<32sec) patches. Scale bars in all panels are 5 µm. Associated with **Movie 2**.

the Nwk^{SH3a} domain) might be required for full activation. To test this hypothesis, we asked whether the Nwk^{SH3a} ligand WASp could cooperate with Dap160 to enhance Nwk membrane binding. Strikingly, the addition of $Dap160^{SH3CD}$ and WASp together enhanced Nwk membrane association to the level of the isolated F-BAR domain (**Fig 4A**). Moreover, coordinated binding of all three components resulted in significantly enriched membrane association of both WASp and Dap160 (**Fig 4A**), which we observed directly using fluorescently labeled proteins on GUVs (**Fig 4B**). Consistent with the direct Dap160-Nwk^{SH3b} interaction, we found that deletion of the Nwk^{SH3b} domain abolished both the $Dap160^{SH3CD}$-dependent increase and the coordinated recruitment of WASp and Dap160 (**Fig S4A**). Notably, addition of Dap160 and WASp did not change the nature of membrane deformations generated by Nwk (scalloped and pinched membranes (Becalska et al., 2013)), suggesting that Dap160 and WASp together potentiate rather than alter the inherent activity of Nwk (**Fig 4C**). These data indicate that Dap160-Nwk SH3-mediated interactions potentiate Nwk association with membranes *in vitro* and at synapses.

Similar its effect on Nwk membrane binding, we also observed that $Dap160^{SH3CD}$ enhanced Nwk-WASp mediated actin assembly, using pyrene-actin assembly assays (**Fig 5**). The combination of Nwk and $Dap160^{SH3CD}$ significantly enhanced the rate of WASp-Arp2/3-mediated actin assembly compared to Nwk (**Fig 5A**). This effect is through Nwk, as $Dap160^{SH3CD}$ had no effect on WASp-Arp2/3 alone. Further, Dap160 enhancement of Nwk-WASp actin assembly required the $Dap160^{SH3D}$ domain, further showing that the specific $Dap160^{SH3D}$-$Nwk^{F\text{-}BAR}$ interaction relieves functional Nwk autoinhibition *in vitro*.

We previously showed that Nwk autoinhibition persists even when associated with membranes. To test whether Dap160 could relieve this persistent autoinhibition, we measured WASp-Arp2/3 actin assembly in reactions containing Dap160, Nwk, and $PI(4,5)P_2$-rich liposomes (**Fig 5B**). Indeed, $PI(4,5)P_2$ containing liposomes synergistically activated WASp-mediated actin assembly in concert with Dap160 and Nwk. By contrast, neither Nwk, $PI(4,5)P_2$, or Nwk+$PI(4,5)P_2$ on their own were sufficient to activate WASp above baseline (**Fig 5B**). Since $PI(4,5)P_2$ is insufficient to robustly activate either WASp or Nwk under these conditions (Stanishneva-Konovalova et al., 2016), our data suggest that WASp activation reflects coordinated relief of Nwk autoinhibition by Dap160 and membranes. Finally, to further explore the coupling between lipid association and actin assembly, we conducted F-actin assembly assays in a droplet format, in which protein-containing aqueous droplets are surrounded by a lipid interface, with lipid head groups directly contacting the aqueous phase (**Fig 5C**). In this assay, we found that coordinated interactions among Nwk, Dap160, and WASp directed actin assembly to the lipid interface. By contrast, substitution of Nwk lacking its autoinhibitory and Dap160-interacting SH3b domain ($Nwk^{\Delta SH3b}$) caused actin to assemble as free floating asters (**Fig 5C**). We previously found that expression of a similarly deregulated fragment ($Nwk^{1\text{-}631}$) at the NMJ led to diffuse actin filament assembly throughout the synapse (Stanishneva-Konovalova et al., 2016). Together with our *in vitro* data in aqueous droplets (**Fig 5C**), this suggests that Nwk^{SH3b} has a dual role of maintaining autoinhibition via Nwk-F-BAR interactions and directing actin assembly to specific synaptic locations via Dap160-mediated activation.

Dap160-Nwk interactions regulate synaptic F-actin patch dynamics

To determine how these mechanisms direct WASp-mediated actin assembly at the synapse, we measured actin dynamics in *nwk* (**Fig 6A-F**) and *dap160* (**Fig 6G-I**) mutant NMJs. Based on our *in vitro* results, we predicted two possible outcomes based on the dual roles of the Nwk-Dap160-WASp module: On the one hand, mutations in these WASp regulators might diminish patch frequency, duration, or intensity (if required for initiation or maturation of patches). Alternatively, the "clamping" function provided by Nwk autoinhibition might prevent spurious or unproductive patch assembly. We first imaged actin dynamics at 15 frames per minute over 6 minutes, to detect a wide range of possible dynamics (detection range 16 to >300 sec). Notably, both mutants exhibited an identical effect on synaptic actin patches: loss of either Nwk or Dap160 significantly increased the abundance of very short-lived (16-30 sec) patches (**Fig 6B,H**). To analyze this shorter-lived population with greater precision, we compared control and *nwk* mutant larvae by imaging at 1Hz. This method only captures short-lived events, both because long events are unlikely to fall entirely within the imaging window, and are also more likely to be excluded due to brief failed detections (see methods). With this analysis, we found that the frequency of short-lived patches (<32 seconds) was significantly higher in *nwk* mutants, consistent with an increase in this population (**Fig 6F**). We did not find a difference in the distribution of patch lifetimes using this method, suggesting that it is the frequency of short events, and not their duration *per se*, that changes (**Fig 6E**). Importantly, the loss of the $Dap160^{SH3CD}$ domains caused the identical shift in patch frequency to the *nwk* and *dap160* loss of function mutants (**Fig 6J-L**) , demonstrating that this phenotype is specific to the domain interactions required for release of Nwk from autoinhibition *in vitro* (**Fig 3A-B, Fig 5A-B**). Together with partial defects in membrane uptake in our experiments (see **Fig 7** below) and in other PAZ mutants (Dickman et al., 2006; Koh et al., 2007), we conclude that these altered F-actin dynamics are not productive endocytic events. Thus, Dap160-Nwk interactions are required to constrain spurious, non-productive actin assembly at synapses, consistent with their combined activity *in vitro*.

Synaptic F-actin patches are likely sites of endocytosis

We next investigated the physiological functions of Dap160-Nwk control of synaptic F-actin dynamics. We first asked whether synaptic F-actin patches represented sites of endocytosis. Since clathrin-mediated endocytosis (CME) is the dominant mode of synaptic vesicle retrieval at this synapse (Heersen et al, 2008, Kasprowicz et al. 2008), we examined the localization of the clathrin adapter AP2α. AP2α accumulated in discrete puncta (**Fig 7A-C**) more numerous than expected given the rate of vesicle release at this synapse (Akbergenova et al., 2018; Melom et al., 2013) (~7 spontaneous release events/10μm^2/min) and the expected duration of a compensatory CME event (~1 min). This suggests that most PAZ-AP2α puncta are not actively engaged in compensatory endocytosis, and may represent structures poised for membrane internalization. By contrast, the frequency of actin patches is much closer to the expected rate of compensatory endocytosis (**Fig S1G**). Further, a majority of actin patches colocalized with AP2α::GFP (**Fig 7B**, Manders' M1 = 0.59+/-.09) in single live images, and we observed dynamic colocalization of individual AP2α and lifeact puncta (**Fig 7C**), consistent with a role in endocytosis.

We then asked how mutations in Nwk and Dap160 that perturb F-actin patch dynamics affect synaptic endocytosis, by measuring FM dye uptake (**Fig 7D-G**). *nwk*$^{1/2}$ null mutants led to a ~66% decrease in FM4-64fx uptake compared to controls (**Fig 7D-E**), an intermediate phenotype compared to dominant negative dynamin in *shi*^{1} mutants (FM uptake 28% of controls). Dap160 null mutants have been previously shown to exhibit an endocytosis defect (Koh et al., 2004; Marie et al., 2004), so we next tested whether the interaction between Dap160 and Nwk is required to support normal endocytosis. Indeed, we found that rescue of *dap160* null mutants with Dap160$^{\Delta SH3CD}$ also significantly diminished FM dye uptake (73% of Dap160^{FL} rescue controls, **Fig 7F-G**) to a similar extent as loss of *nwk*. By contrast, loss of the Dap160^{SH3D} domain alone caused no defects in FM uptake, consistent with the lack of effect of this mutation on Nwk accumulation and localization (**Fig 2E-G**). Finally, as both Nwk and Dap160 are implicated in the trafficking of synaptic growth-promoting BMP receptors (O'Connor-Giles 2008, Rodal 2008), we tested whether the Dap160-Nwk interaction was required for normal synaptic growth, which we assayed by counting satellite boutons, a hallmark phenotype of both null mutants. Surprisingly, we found that both Dap160$^{\Delta SH3D}$ or Dap160$^{\Delta SH3CD}$ truncations were able to rescue satellite bouton numbers to wild type levels (**Fig S5A**), suggesting that Dap160 and Nwk might contribute to synaptic growth in parallel pathways, or that additional ligands are able to support the growth-regulatory activities of Nwk and Dap160. Overall, our data suggest the Dap160-Nwk interaction is required for normal synaptic vesicle endocytosis, and together with the finding that Dap160 and Nwk regulate actin patch dynamics support the hypothesis that actin patches represent active endocytic events.

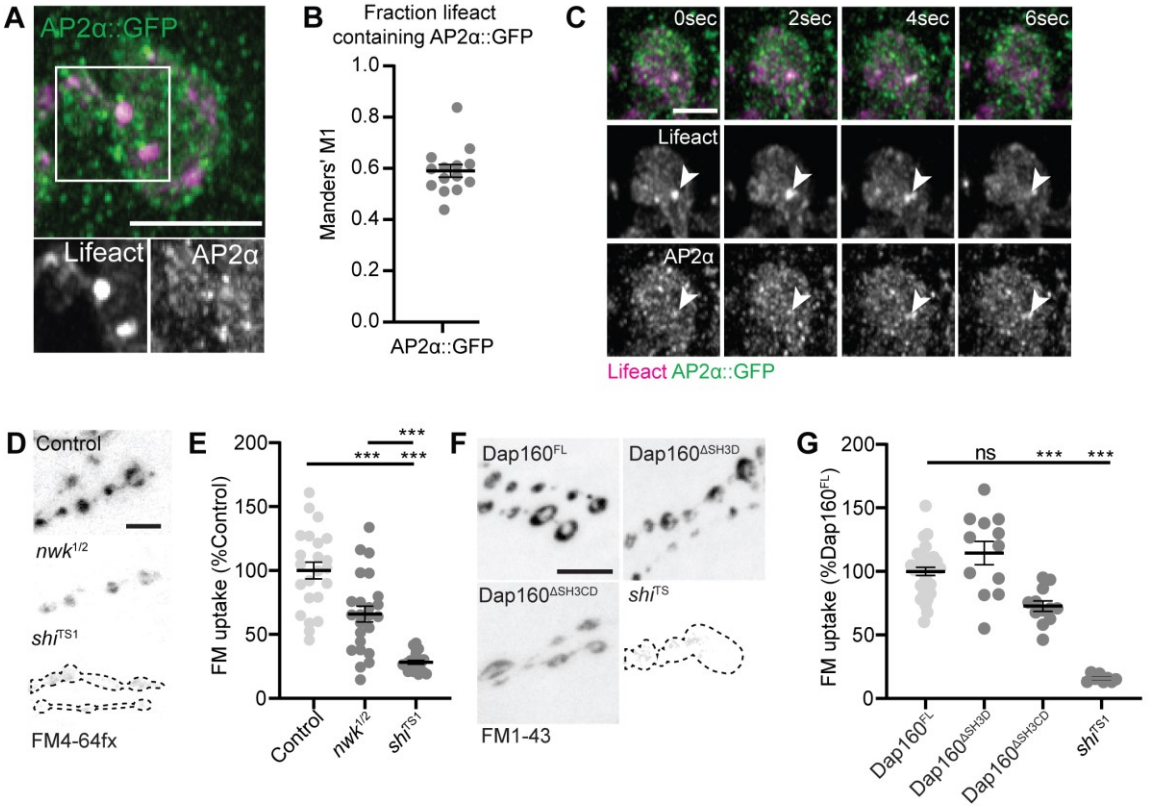

Figure 7. Actin patches are likely sites of synaptic endocytosis. (A) Images show maxIPs of Airyscan micrographs of single frames of muscle 6/7 NMJs expressing lifeact::ruby (magenta, left inset) and AP2α::GFP (green, right inset). A majority of actin patches colocalize AP2α::GFP. (B) Quantification of colocalization by Manders' coefficients. M1 represents % of lifeact region that contains α::GFP signal above threshold. (C) Timelapse showing dynamic colocalization of Lifeact::Ruby actin patches with AP2α ::GFP. (D-G) FM dye uptake assays at m6/7 NMJs following 5 min 90mM potassium stimulation at 36ºC. (D,F) maxIPs of spinning disc confocal micrographs of FM dye uptake assays. (D-E) *nwk* mutants exhibit partially defective FM4-64fx dye uptake, compared to *shi*^{TS1} mutants. (F-G) Loss of Dap160-Nwk interactions in a Dap160$^{\Delta SH3CD}$ truncation (but not Dap160$^{\Delta SH3D}$) exhibit partially defective FM1-43 dye uptake relative to *shi*TS1, similar to *nwk* mutants. Graphs show mean +/- s.e.m. ; n represents NMJs. Scale bars are 5 µm (E,G) or 2.5 µm (F). Associated with **Fig S5**.

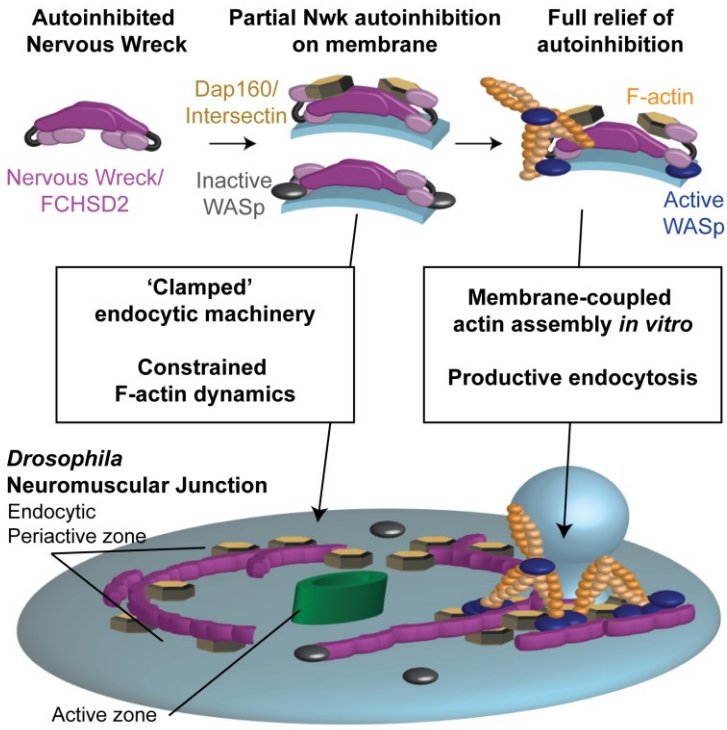

Figure 8. Autoinhibition clamps PAZ-mediated synaptic F-actin assembly. Coordinated binding with Dap160 and WASp at negatively charged membranes relieves Nwk autoinhibition of membrane-associated actin assembly *in vitro* (top). Autoinhibitory clamp prevents spurious actin assembly, while coordinated relief from autoinhibition drives productive endocytic actin assembly at the *Drosophila* NMJ (bottom).

Discussion

Here we identify a mechanism by which autoinhibition clamps the presynaptic endocytic machinery to regulate the dynamics of discrete synaptic actin assembly events and the efficiency of synaptic endocytosis. We identify specific interactions among Nwk, Dap160, and WASp that function in two ways to potentiate membrane associated actin dynamics: 1) Persistent autoinhibition of Nwk allows for stable binding of inactive PAZ machinery to presynaptic membranes to constrain spurious actin assembly events. 2) Coordinated relief of Nwk autoinhibition by Dap160 and WASp robustly activate F-actin assembly and ensure that actin assembles into structures that are likely to productively remodel membranes. This provides a mechanism by which synapses can use the micron-scale PAZ organization of endocytic machinery to efficiently generate 50-100 nm-scale endocytic events, in response to physiological cues such as synaptic transmission.

The predominant presynaptic actin structures resemble endocytic patches

Here we provide the first quantitative analysis of the composition and dynamics of individual presynaptic F-actin structures. Numerous studies have examined actin dynamics at the level of entire synapses or qualitatively described dynamics of discrete actin structures (Bloom et al., 2003; Colicos et al., 2001; Nunes et al., 2006; Piccioli and Littleton, 2014; Sankaranarayanan et al., 2003), and identified diverse roles for actin, including synaptic vesicle endocytosis (Holt et al., 2003; Kononenko et al., 2014; Soykan et al., 2017; Watanabe et al., 2013; Wu et al., 2016), synaptic vesicle organization and mobilization (Guzman et al., 2019; Lee et al., 2012; Marra et al., 2012; Owe et al., 2009; Sakaba and Neher, 2003; Wolf et al., 2015), active zone organization and function (Boyl et al., 2007; Morales et al., 2000; Wagh et al., 2015; Waites et al., 2011; Wang et al., 1999), and receptor mediated endocytosis (Kim et al., 2019; Rodal et al., 2008). Bulk analyses, which do not separate individual dynamic actin structures in space and time, are limited in their ability to discern how the regulation and dynamics of actin contribute to these distinct functions. We leveraged our ability to extract data describing individual structures to find that synaptic actin predominantly assembled into discrete Arp2/3-associated patches, and identified points of control over their dynamics. Specifically, we found that loss of endocytic proteins differentially affected the frequency and kinetics of individual actin patches, which correlate with functional deficits in endocytosis.

The link between the actin structures that we observe and endocytic events is supported by several lines of evidence: the morphology and duration of synaptic actin patches are similar to WASp/Arp2/3-dependent endocytic dynamics in mammalian cells (Doyon et al., 2011; Grassart et al., 2014; Merrifield et al., 2004), and their frequency approaches the rate of spontaneous synaptic vesicle release at this synapse (**Fig S1G**) (Melom et al., 2013, Akbergenova 2018); the same endocytic proteins and protein interactions that regulate endocytosis at this synapse also alter the dynamics of actin patches; and patches colocalize partially with endocytic adapters. Technical challenges due to the high density of endocytic proteins and cargoes, and the difficulty of conducting sparse single vesicle measurements at this synapse (compared to neurons in culture (Chanaday and Kavalali, 2018; Peng et al., 2012)) make it difficult to directly link the dynamics of actin structures to specific membrane remodeling and cargo uptake events. However, the frequency of the events captured by our approach makes it unlikely that they represent rarer F-actin-dependent events at this synapse, such as those that control macropinocytosis or new bouton growth (Khuong et al., 2010; Kim et al., 2019; Piccioli and Littleton, 2014).

Autoinhibition clamps PAZ membrane remodeling machinery at synapses

Our data demonstrate that much of the synaptic membrane remodeling machinery is held in an inactive state at the presynaptic membrane: Nwk and Dap160 accumulate in a micron-scale membrane domain (**Figs 1A, S1A, 3C**), and loss of this machinery increases the frequency of short-lived actin patches (**Fig 6**). Together with our prior *in vitro* findings (Stanishneva-Konovalova et al., 2016), these data suggest that these PAZ proteins are held in a primed, partially autoinhibited state at the membrane *in vivo*. The fact that loss of Nwk increases the frequency of short patches while decreasing FM uptake suggests that the actin structures assembled in the *nwk* mutant are unproductive for synaptic vesicle endocytosis. These spurious patches could reflect non-specific actin assembly, perhaps due to unmasking of the Nwk ligand PI(4,5)P_2 at the membrane and/or inappropriate activation of alternative WASp-dependent actin assembly pathways. Indeed, additional WASp activators such as Snx9 and Toca-1 may play accessory roles in endocytic actin assembly (Almeida-Souza et al., 2018; Gallop et al., 2013), consistent with our finding that loss of presynaptic WASp led to a decrease in the total number of patches (**Fig 1E-G, Fig SS1D-F**). Our data indicate that at the synapse, where endocytic machinery accumulates at high concentrations (Wilhelm et al., 2014) and recruitment appears uncoupled from activation, these layers of autoregulation are critical to constrain actin assembly generally.

Our findings on autoinhibition and clamping connect two prevailing models of the organization and function of the synaptic endocytosis machinery- preassembly and delivery. In the first model, preassembly of clathrin and accessory proteins is hypothesized to ensure fast endocytosis in response to synaptic vesicle fusion (Hua et al., 2011; Mueller et al., 2004; Wienisch and Klingauf, 2006). Here, Nwk autoinhibition provides a mechanism to assemble an inactive, yet poised endocytic apparatus. In the second model, endocytic adapters associate with the synaptic vesicle pool, providing a ready source or buffer of proteins that can be released upon calcium signaling or vesicle fusion (Bai et al., 2010; Denker et al., 2011; Gerth et al., 2017; Winther et al., 2015). As Dap160/Intersectin releases Nwk from autoinhibition and has been shown to shuttle between the synaptic vesicle pool and the plasma membrane, it could serve as a single activator that couples the preassembly and delivery models.

Coordinated relief of autoinhibition potentiates membrane-associated actin dynamics

Our *in vitro* data show that beyond functioning as a clamp, Nwk and Dap160 collaboratively activate WASp to promote robust actin assembly. Together with the defects we observed *in vivo* for actin dynamics and FM dye uptake, these data suggest that Dap160-Nwk-WASp interactions could serve as a coincidence detection mechanism to relieve autoinhibition of Nwk and promote productive actin assembly. Coincidence detection mechanisms for F-actin assembly have been demonstrated in several models of endocytosis (Case et al., 2019; Sun et al.), suggesting that amplification of WASp membrane binding could drive robust actin patch assembly at synapses. Similarly, in human cells, the interaction between FCHSD2, Intersectin, and WASp promotes actin assembly and endocytic maturation (Almeida-Souza et al., 2018) or initiation (Xiao et al., 2018). The Dap160-Nwk module could act by directing and/or organizing actin assembly specifically at endocytic events, akin to the membrane directed actin assembly we observed *in vitro* (**Fig 6C**), and/or ensure that it is sufficiently robust for productive membrane remodeling (Akamatsu et al., 2020), consistent with our pyrene actin assays and the increased frequency of short duration actin assembly events. Direct support for these models will require new analytical or imaging approaches to directly visualize the coupling of membranes and actin to the endocytic machinery, in order to distinguish spurious (due to unclamping) vs bona fide but underpowered endocytic actin assembly events.

Physiological implications of autoregulatory mechanisms in the periactive zone

Our data suggest that the endocytic machinery could be deployed as clamped, primed, or activated complexes at different locations at the synapse. The next critical step will be to determine how physiological cues such as calcium influx or synaptic vesicle release might recruit or activate Dap160 or WASp to regulate transitions between these states. One intriguing possibility is that these mechanisms might enable an endocytic periactive zones to locally regulate, respond, or adapt to the release properties of their locally associated active zones (Akbergenova et al., 2018; Melom et al., 2013), and serve as novel points of control over synaptic plasticity and homeostasis.

Materials and Methods

RESOURCE AVAILABILITY

Lead Contact

Further information and requests for resources and reagents should be directed to and will be fulfilled by the Lead Contact, Avital Rodal (arodal@brandeis.edu).

Materials Availability

All plasmids and fly lines generated in these studies are available upon request.

Data and Code Availability

All custom FIJI/ImageJ and Python scripts used to analyze the data in these studies are available upon request.

EXPERIMENTAL MODEL DETAILS

***Drosophila* culture:** Flies were cultured using standard media and techniques. All flies were raised at 25º C, with the exception of experiments using Dcr2; Dap160 RNAi or WASp RNAi, for which flies were raised at 29º C. See key resources table for all fly lines used and see Supplemental Table 1 for full experimental genotypes of each experiment in this study.

METHODS DETAILS

Cloning: UAS-Dap160 constructs were generated in pBI-UASC-mCherry (derived from (Wang et al., 2011), see (Deshpande et al., 2016)). Fragments were amplified from the genomic Dap160 locus with primers described in the key resources table. These transgenes were injected into flies (Rainbow Gene), using ΦC31-mediated integration at the Attp40 locus (Ni et al., 2008), to ensure that all constructs were in a similar genomic context. UAS-WASp-tev-myc was generated in pUAST (Brand and Perrimon, 1993) by inserting a TEV recognition site and 9 copies of the myc epitope tag at the 3' end of the Wsp cDNA, and injected into w^{1118} flies at the Duke Model Systems Transgenic Facility (Duke University, Durham, NC).

Generation of AP2α-GFP^{KI}: The vector pHD-sfGFP-dsRed was created using Gibson assembly by amplifying sfGFP from pScarlessHD-sfGFP-DsRed (gift from Kate O'Connor-Giles, Addgene plasmid # 80811) and inserting it in between the multiple cloning site and the first loxP site in the pHD-DsRed backbone (gift from Kate O'Connor-Giles, Addgene plasmid # 51434). 1 kb sequences upstream and downstream of the stop codon were amplified from the genomic locus of AP2α and inserted into pHD-sfGFP-dsRed using AarI and SapI, respectively, to create the HDR donor pMM007_pHD-AP2a-C-sfGFP-dsRed. The guide RNA GGAAATCTGCGATCTGTTGA was cloned into pU6-BbsI-chiRNA (gift from Melissa Harrison & Kate O'Connor-Giles & Jill Wildonger, Addgene plasmid # 45946 (Gratz et al., 2013); using BbsI to create pMM008_pU6-AP2a-chiRNA. 500 ng/uL HDR donor plasmid and 100 ng/uL gRNA plasmid were injected into vas-Cas9(III) flies (BDSC 51324, injections by BestGene). Correct integration of the transgene was validated by sequencing.

FM dye uptake: FM dye (FM1-43 in *dap160* experiments, or FM4-64FX in *nwk* experiments) uptake experiments were performed essentially as described (Ramachandran and Budnik, 2010; Verstreken et al., 2008). For fixed experiments (*nwk* mutants), larvae were dissected in groups of 4-6 (with each dish having at least two control larvae) in low-calcium HL3 (Stewart et al., 1994), and axons were cut to dissociate CNS input. For live imaging (*dap160* rescues), larvae were dissected, stained, and imaged in pairs, with one control ($Dap160^{FL}$) and one experimental larva per dish. In both sets of experiments, dye loading (4 µM) was performed in 90 mM KCl, 2 mM $CaCl_2$ HL3 saline for five minutes at 36°C on a submerged metal block using prewarmed buffer. This temperature has been shown to exacerbate endocytic defects in some mutants, including *dap160* (Koh et al., 2004). Following extensive washing in Ca^{++} free saline, larvae were fixed in 4% paraformaldehyde in Ca^{++} free saline (for *nwk* experiments) or imaged live (for *dap160* transgene rescue experiments). Images of muscle 6/7 NMJs (abdominal segments 3-5) were acquired by confocal microscopy and FM dye intensity was measured within mCherry (in *dap160* experiments) or GFP (in *nwk* experiments)-labeled presynaptic masks, and intensities were normalized to dish-matched control larvae.

Immunohistochemistry: For analysis of NMJ morphology and protein localization, flies were cultured at low density at 25°C. Wandering third instar larvae were dissected in calcium-free HL3.1 saline (Feng et al., 2004) and fixed for 30 min in HL3.1 containing 4% formaldehyde. For analysis of NMJ overgrowth (satellite boutons), samples were stained with anti-HRP and anti-Dlg, and images were blinded before manual bouton counting. Boutons were counted on muscle 4 NMJs, abdominal segments 2-4, and satellite boutons were defined as any string of fewer than five boutons that branched from the main NMJ branch (O'Connor-Giles et al., 2008).

Western blots: *Drosophila* heads (10 pooled/genotype) were homogenized in 100 µL 2x Laemmli buffer. 10uL of extract per lane were fractionated by SDS/PAGE and immunoblotted with α-Dap160 (Roos 1998) and α-Tubulin antibodies (clone B-5-1-2, Sigma).

Imaging and analysis: Spinning-disk confocal imaging of *Drosophila* larvae was performed at room temperature on a Nikon Ni-E upright microscope equipped with 60× (NA 1.4) and 100× (NA 1.45) oil immersion objectives, a Yokogawa CSU-W1 spinning-disk head, and an Andor iXon 897U EMCCD camera. Images were collected using Nikon Elements AR software.

FRAP data (**Fig 3C**) were acquired on a Zeiss 880 with Airy Scan in super resolution acquisition mode, using a 63X NA1.4 objective. Single Z-slices through the middle of individual boutons were acquired at 4Hz for 90sec, with manual focus adjustment. Following acquisition of two or three initial Z-stacks to assess prebleach intensity, <~20% of individual boutons were photobleached by the 488 laser at .6 intensity and scan speed of 6. Intensities of background, unbleached, and bleached ROIs were acquired manually using FIJI, and bleached area was normalized to prebleach and unbleached ROIs (to correct for imaging-induced photobleaching), and analyzed with GraphPad Prism.

Confocal imaging of GUVs and cell-sized water droplets was conducted at room temperature on a Marianas spinning disk confocal system (3I, Inc, Denver,CO), consisting of a Zeiss Observer Z1 microscope equipped with a Yokagawa CSU-X1 spinning disk confocal head, a QuantEM 512SC EMCCD camera, PLAN APOCHROMAT 63X or 100x oil immersion objectives (n.a. 1.4), a Photonics Instruments Micropoint photo-ablation device, and Slidebook software.

Super-resolution images of protein localization in fixed samples were acquired with a Nikon SIM-E system, consisting of an inverted Eclipse Ti-E microscope, 100x (n.a 1.45) oil-immersion objective, and Hamamatsu OrcaFLASH4 CMOS camera. Images were acquired at room temperature as Z-stacks using a regime of 3 grid orientations and 5 phases. Channels were registered using Tetraspeck beads (ThermoFisher), and SIM reconstruction was performed using Nikon Elements software. Super-resolution images of protein localization in live samples were acquired with a Zeiss 880FAS microscope in fast Airyscan mode with a 63X (NA1.4) oil immersion objective, using Zen Blue software.

Analysis of actin dynamics at the NMJ*:* Spinning disk confocal time series were acquired at 15 stacks/min, except for experiments in Fig 6D-F, which were acquired at 60 stacks/min. A maximum intensity projection was made of each time point, movies were registered using the FIJI plugin StackReg, and analyzed by Patchtracker (Berro and Pollard, 2014) as follows: The threshold for patch detection was normalized to the mean probe intensity in the presynaptic area (threshold=Probe Mean * 0.40). All other settings for patch detection and tracking were default: Estimated patch diameter .6µm, median filter=false, subpixel detection=true. Linking max distance=.5µm, Gap-closing distance=.5 µm, Gap-closing frame gap=0. For .25Hz imaging experiments, patches between 16-356s could be detected. For 1Hz imaging experiments, patches between 4-139s could be detected.

Intensity and Colocalization analysis: For intensity and colocalization, the presynaptic region was masked in 3D using a presynaptically enriched label: either HRP (Fig 3E, S4B), Nwk (Fig 1C, S1A, 3F), Dap160 (S1B), or Lifeact::ruby (Fig 2B). For mask generation, images were subjected to a gaussian blur filter and thresholded by intensity. Blur radius and the specific threshold algorithms used were empirically optimized for each experiment to consistently and accurately reflect the presynaptic area in control and mutant groups (and the same settings were used for all NMJs within any given experiment). Signal intensities were measured in 3D using a FIJI script, and colocalization analysis was performed in 3D on Airyscan or SIM reconstructed image stacks using the Coloc2 plugin for ImageJ (https://imagej.net/Coloc_2). For all images, background was subtracted using the rolling ball method with a radius of 50 pixels.

In vitro assays

Protein purification: $Dap160^{SH3C}$ and $Dap160^{SH3CD}$ were amplified from Dap160 Isoform A and cloned into pTrcHisA (see STAR methods for details). N-terminally His-Xpress–tagged proteins (Nwk^{1-633}, Nwk^{1-731}, $Nwk^{607-731}$, Nwk^{1-428}, $Wsp^{143-529}$, $Dap160^{SH3C}$, $Dap160^{SH3CD}$), were purified as described previously(Becalska et al., 2013; Kelley et al., 2015; Rodal et al., 2008; Stanishneva-Konovalova et al., 2016). In brief, proteins were purified from BL21(DE3) Escherichia coli using cobalt or nickel columns, followed by ion exchange and gel filtration into 20 mM Tris pH 7.5, 50 mM KCl, 0.1 mM EDTA, and 0.5 mM DTT. GST fusions ($Dap160^{SH3CD}$, $Dap160^{SH3C}$, $Dap160^{SH3D}$) were amplified from Dap160 isoform A and cloned into pGEX4t (see STAR methods for details). Proteins were purified with glutathione agarose (Thermo Scientific, Waltham MA) in 20 mM Tris 7.5, 20 mM KCl, and 0.5 mM dithiothreitol (DTT) supplemented with protease inhibitors (P2714 (Sigma-Aldrich, St. Louis, MO) and 0.5 mg/mL pepstatin A). Arp2/3 complex was purchased from Cytoskeleton, Inc. Actin was purified from from acetone powder (Spudich and Watt, 1971) generated from frozen ground hind leg muscle tissue of young rabbits (PelFreez, Rogers, AR).

Coprecipitation assays: Coprecipitation with GST-tagged proteins were conducted as described previously (Kelley et al., 2015): Concentrations of GST fusions on beads were normalized using empty beads and bead volume was restricted to two-thirds of the total reaction volume. GST fusions were incubated with agitation with His-tagged target proteins at room temperature for one hour in binding buffer (20 mM Tris pH 8.0, 20 mM KCl, 0.5 mM DTT). For salt sensitivity experiments, the indicated concentrations of NaCl were used in place of KCl in the binding buffer. Beads were then pelleted and washed once with buffer after removing the supernatant. Pellets and supernatants were then boiled in Laemmli Sample Buffer and fractionated by SDS-PAGE, followed by Coomassie staining or immunoblotting as noted in figure legends, followed by imaging and analysis on a LICOR Odyssey device.

Lipsome cosedimentation: Lipid cosedimentation assays were conducted as described previously (Becalska et al., 2013). In brief, liposomes were swelled from dried lipid films in 20 mM Hepes pH 7.5 and 100 mM NaCl. Specific lipid compositions are indicated in the figure legends. Proteins were then mixed with 1 mg/mL liposomes, incubated for 30 min at room temperature, and then pelleted for 20 min at 18,000 × g at 4 °C. Pellets and supernatants were then denatured in Laemmli sample buffer and fractionated by SDS/PAGE, followed by Coomassie staining, and imaging and analysis on a LICOR Odyssey device.

GUV decoration: GUVs were generated by gentle hydration. Briefly, 10 µL of 10 mg/mL lipids dissolved in 19:1 chloroform:methanol were dried under vacuum, then swelled in 300 µL of 5 mM HEPES 300 mM sucrose, pH 7.5 overnight at 70ºC. GUVs were imaged on a Marianas spinning disk confocal system (see above). 3 µL GUVs were diluted into 5 mM HEPES 150 mM KCl pH7.5, incubated with protein as noted in figures, and imaged using a 100X/ N.A. 1.4 objective in multiwell slides (Lab-Tek) precoated with 1 mg/mL BSA. After a 30 min incubation, 1% agarose in 5 mM HEPES 150 mM KCl pH 7.5 was added (final agarose concentration .5%) to limit GUV mobility. Images were analyzed by line tracing intensity profiles across a medial optical section of GUVs.

Actin assembly in droplets: Lipids (97.5% DPHPC [1,2-diphytanoyl-sn-glycero-3-phosphocholine], Avanti Polar Lipids) and 2.5% $DPHPC:PI(4,5)P_2$) were mixed in chloroform, dried under vacuum, and rehydrated to 23 mM (20 mg/ml) in decane. The indicated proteins were added to the lipid mix at a 1:50 volume ratio and pipetted vigorously until cloudy before imaging by spinning disk confocal microscopy.

Pyrene-actin assembly: Rabbit muscle actin [5% (mol/mol) pyrene-labeled] was gel-filtered, prespun at 90,000 x g, exchanged from Ca^{2+} to Mg^{2+}, and assembled at a final concentration of 2.5 µM as described previously (Moseley et al., 2006). Proteins were preincubated with 74 µg/mL liposomes or control buffer for 30 min before actin assembly reactions. Assembly was monitored with a spectrofluorometer (Photon Technology International) using an excitation wavelength of 365 nm and an emission wavelength of 407 nm. Rates were calculated from slopes of

curves in the linear range, and curves were plotted using GraphPad Prism software.

QUANTIFICATION AND STATISTICAL ANALYSIS

Graphs were prepared and statistical analyses performed using Graphpad Prism software. For normally distributed data, comparisons were made using either T-test or ANOVA with posthoc Bonferroni's multiple comparisons test. For non-normally distributed data, comparisons were made using either Mann-Whitney U test, or Kruskal-Wallis test with posthoc Dunn's test. Please see Supplemental Table 1 for each statistical test performed for each experiment presented in this study. Comparison of patch duration distributions was performed using a Kolmogorov-Smirnoff test. All data are shown as the mean +/- SEM.

Author Contributions and Notes

Conceptualization S.J.D, C.F.K, E.M.M, A.A.R. Methodology S.J.D, C.F.K, E.M.M, A.A.R. Software S.J.D. Formal Analysis S.J.D, C.F.K, M.F.M, E.M.M. Investigation S.J.D, C.F.K, E.M.M, T.L, M.F.M, B.E. Resources C.F.K, E.M.M, T.L, M.M, M.K. Data curation S.J.D, C.F.K, E.M.M, A.A.R. Writing – Original Draft S.J.D, C.F.K, A.A.R. Writing – Review & Editing S.J.D, C.F.K, B.E, M.M, M.K, A.A.R. Visualization S.J.D, C.F.K, A.A.R. Supervision M.K, A.A.R. Project Administration A.A.R. Funding Acquisition M.K, A.A.R.

The authors declare no conflict of interest.

This article contains supporting information online.

Acknowledgments

The authors would like to thank Bruce Goode for actin reagents and and advice, Julien Berro for particle tracking advice, Oleg Shupliakov for helpful discussions, Graeme Davis for anti-Dap160 antibody, and the Bloomington *Drosophila* Stock Center (Indiana University, Bloomington, IN, NIH P40OD018537) for providing fly stocks;. This work was supported a Basil O'Connor Scholar Award from the March of Dimes, a Pew Scholar award, and the Brandeis NSF MRSEC, Bioinspired Soft Materials (NSF-DMR 1420382) (AAR); by T32 NS007292 (SJD), T32 GM007122 (CFK), and R90 DA03243501 (MFM); and by the Swiss National Science Foundation (grant 310030B_182825) and NCCR Chemical Biology funded by the SNSF (MK, MM).

References

Akamatsu, M., Vasan, R., Serwas, D., Ferrin, M.A., Rangamani, P., and Drubin, D.G. (2020). Principles of self-organization and load adaptation by the actin cytoskeleton during clathrin-mediated endocytosis. eLife *9*, e49840.

Akbergenova, Y., Cunningham, K.L., Zhang, Y.V., Weiss, S., and Littleton, J.T. (2018). Characterization of developmental and molecular factors underlying release heterogeneity at *Drosophila* synapses. elife *7*.

Almeida-Souza, L., Frank, R.A.W., García-Nafría, J., Colussi, A., Gunawardana, N., Johnson, C.M., Yu, M., Howard, G., Andrews, B., Vallis, Y., et al. (2018). A Flat BAR Protein Promotes Actin Polymerization at the Base of Clathrin-Coated Pits. Cell *174*, 325-337.e14.

Bai, J., Hu, Z., Dittman, J.S., Pym, E.C.G., and Kaplan, J.M. (2010). Endophilin functions as a membrane-bending molecule and is delivered to endocytic zones by exocytosis. Cell *143*, 430–441.

Becalska, A.N., Kelley, C.F., Berciu, C., Stanishneva-Konovalova, T.B., Fu, X., Wang, S., Sokolova, O.S., Nicastro, D., and Rodal, A.A. (2013). Formation of membrane ridges and scallops by the F-BAR protein Nervous Wreck. Mol Biol Cell *24*, 2406–2418.

Ben-Yaacov, S., Le Borgne, R., Abramson, I., Schweisguth, F., and Schejter, E.D. (2001). Wasp, the *Drosophila* Wiskott-Aldrich syndrome gene homologue, is required for cell fate decisions mediated by Notch signaling. J. Cell Biol. *152*, 1–13.

Berro, J., and Pollard, T.D. (2014). Local and global analysis of endocytic patch dynamics in fission yeast using a new "temporal superresolution" realignment method. Mol. Biol. Cell *25*, 3501–3514.

Bloom, O., Evergren, E., Tomilin, N., Kjaerulff, O., Löw, P., Brodin, L., Pieribone, V.A., Greengard, P., and Shupliakov, O. (2003). Colocalization of synapsin and actin during synaptic vesicle recycling. The Journal of Cell Biology *161*, 737–747.

Boyl, P.P., Nardo, A.D., Mulle, C., Sassoè-Pognetto, M., Panzanelli, P., Mele, A., Kneussel, M., Costantini, V., Perlas, E., Massimi, M., et al. (2007). Profilin2 contributes to synaptic vesicle exocytosis, neuronal excitability, and novelty-seeking behavior. The EMBO Journal *26*, 2991–3002.

Brand, A.H., and Perrimon, N. (1993). Targeted gene expression as a means of altering cell fates and generating dominant phenotypes. Development *118*, 401–415.

Case, L.B., Zhang, X., Ditlev, J.A., and Rosen, M.K. (2019). Stoichiometry controls activity of phase-separated clusters of actin signaling proteins. Science *363*, 1093–1097.

Chanaday, N.L., and Kavalali, E.T. (2018). Optical detection of three modes of endocytosis at hippocampal synapses. elife *7*.

Colicos, M.A., Collins, B.E., Sailor, M.J., and Goda, Y. (2001). Remodeling of Synaptic Actin Induced by Photoconductive Stimulation. Cell *107*, 605–616.

Collins, A., Warrington, A., Taylor, K.A., and Svitkina, T. (2011). Structural Organization of the Actin Cytoskeleton at Sites of Clathrin-Mediated Endocytosis. Current Biology *21*, 1167–1175.

Coyle, I.P., Koh, Y.-H., Lee, W.-C.M., Slind, J., Fergestad, T., Littleton, J.T., and Ganetzky, B. (2004). Nervous wreck, an SH3 adaptor protein that interacts with Wsp, regulates synaptic growth in *Drosophila*. Neuron *41*, 521–534.

Denker, A., Kröhnert, K., Bückers, J., Neher, E., and Rizzoli, S.O. (2011). The reserve pool of synaptic vesicles acts as a buffer for proteins involved in synaptic vesicle recycling. Proc. Natl. Acad. Sci. U.S.A. *108*, 17183–17188.

Deshpande, M., Feiger, Z., Shilton, A.K., Luo, C.C., Silverman, E., and Rodal, A.A. (2016). Role of BMP receptor traffic in synaptic growth defects in an ALS model. Mol Biol Cell *27*, 2898–2910.

Dickman, D.K., Lu, Z., Meinertzhagen, I.A., and Schwarz, T.L. (2006). Altered Synaptic Development and Active Zone Spacing in Endocytosis Mutants. Current Biology *16*, 591–598.

Doyon, J.B., Zeitler, B., Cheng, J., Cheng, A.T., Cherone, J.M., Santiago, Y., Lee, A.H., Vo, T.D., Doyon, Y., Miller, J.C., et al. (2011). Rapid and efficient clathrin-mediated endocytosis revealed in genome-edited mammalian cells. Nat. Cell Biol. *13*, 331–337.

Evergren, E., Gad, H., Walther, K., Sundborger, A., Tomilin, N., and Shupliakov, O. (2007). Intersectin is a negative regulator of dynamin recruitment to the synaptic endocytic zone in the central synapse. J. Neurosci. *27*, 379–390.

Feng, Y., Ueda, A., and Wu, C.-F. (2004). A modified minimal hemolymph-like solution, HL3.1, for physiological recordings at the neuromuscular junctions of normal and mutant *Drosophila* larvae. J. Neurogenet. *18*, 377–402.

Gallop, J.L., Walrant, A., Cantley, L.C., and Kirschner, M.W. (2013). Phosphoinositides and membrane curvature switch the mode of actin polymerization via selective recruitment of toca-1 and Snx9. Proc. Natl. Acad. Sci. U.S.A. *110*, 7193–7198.

Gerth, F., Jäpel, M., Pechstein, A., Kochlamazashvili, G., Lehmann, M., Puchkov, D., Onofri, F., Benfenati, F., Nikonenko, A.G., Fredrich, K., et al. (2017). Intersectin associates with synapsin and regulates its nanoscale localization and function. Proc. Natl. Acad. Sci. U.S.A. *114*, 12057–12062.

Grassart, A., Cheng, A.T., Hong, S.H., Zhang, F., Zenzer, N., Feng, Y., Briner, D.M., Davis, G.D., Malkov, D., and Drubin, D.G. (2014). Actin and dynamin2 dynamics and interplay during clathrin-mediated endocytosis. J. Cell Biol. *205*, 721–735.

Gratz, S.J., Cummings, A.M., Nguyen, J.N., Hamm, D.C., Donohue, L.K., Harrison, M.M., Wildonger, J., and O'Connor-Giles, K.M. (2013). Genome engineering of *Drosophila* with the CRISPR RNA-guided Cas9 nuclease. Genetics *194*, 1029–1035.

Guerrier, S., Coutinho-Budd, J., Sassa, T., Gresset, A., Jordan, N.V., Chen, K., Jin, W.-L., Frost, A., and Polleux, F. (2009). The F-BAR Domain of srGAP2 Induces Membrane Protrusions Required for Neuronal Migration and Morphogenesis. Cell *138*, 990–1004.

Guzman, G.A., Guzman, R.E., Jordan, N., and Hidalgo, P. (2019). A Tripartite Interaction Among the Calcium Channel α1- and β-Subunits and F-Actin Increases the Readily Releasable Pool of Vesicles and Its Recovery After Depletion. Front Cell Neurosci *13*, 125.

Henne, W.M., Boucrot, E., Meinecke, M., Evergren, E., Vallis, Y., Mittal, R., and McMahon, H.T. (2010). FCHo Proteins Are Nucleators of Clathrin-Mediated Endocytosis. Science *328*, 1281–1284.

Holt, M., Cooke, A., Wu, M.M., and Lagnado, L. (2003). Bulk membrane retrieval in the synaptic terminal of retinal bipolar cells. J. Neurosci. *23*, 1329–1339.

Hua, Y., Sinha, R., Thiel, C.S., Schmidt, R., Hüve, J., Martens, H., Hell, S.W., Egner, A., and Klingauf, J. (2011). A readily retrievable pool of synaptic vesicles. Nature Neuroscience *14*, 833–839.

Jäpel, M., Gerth, F., Sakaba, T., Bacetic, J., Yao, L., Koo, S.-J., Maritzen, T., Freund, C., and Haucke, V. (2020). Intersectin-Mediated Clearance of SNARE Complexes Is Required for Fast Neurotransmission. Cell Reports *30*, 409-420.e6.

Kaempf, N., and Maritzen, T. (2017). Safeguards of Neurotransmission: Endocytic Adaptors as Regulators of Synaptic Vesicle Composition and Function. Front Cell Neurosci *11*, 320.

Kaksonen, M., and Roux, A. (2018). Mechanisms of clathrin-mediated endocytosis. Nat. Rev. Mol. Cell Biol.

Kelley, C.F., Messelaar, E.M., Eskin, T.L., Wang, S., Song, K., Vishnia, K., Becalska, A.N., Shupliakov, O., Hagan, M.F., Danino, D., et al. (2015). Membrane Charge Directs the Outcome of F-BAR Domain Lipid Binding and Autoregulation. Cell Rep *13*, 2597–2609.

Kessels, M.M., and Qualmann, B. (2004). The syndapin protein family: linking membrane trafficking with the cytoskeleton. Journal of Cell Science *117*, 3077–3086.

Khuong, T.M., Habets, R.L.P., Slabbaert, J.R., and Verstreken, P. (2010). WASP is activated by phosphatidylinositol-4,5-bisphosphate to restrict synapse growth in a pathway parallel to bone morphogenetic protein signaling. Proc. Natl. Acad. Sci. U.S.A. *107*, 17379–17384.

Kim, N., Kim, S., Nahm, M., Kopke, D., Kim, J., Cho, E., Lee, M.-J., Lee, M., Kim, S.H., Broadie, K., et al. (2019). BMP-dependent synaptic development requires Abi-Abl-Rac signaling of BMP receptor macropinocytosis. Nat Commun *10*, 684.

Koh, T.-W., Verstreken, P., and Bellen, H.J. (2004). Dap160/intersectin acts as a stabilizing scaffold required for synaptic development and vesicle endocytosis. Neuron *43*, 193–205.

Koh, T.-W., Korolchuk, V.I., Wairkar, Y.P., Jiao, W., Evergren, E., Pan, H., Zhou, Y., Venken, K.J.T., Shupliakov, O., Robinson, I.M., et al. (2007). Eps15 and Dap160 control synaptic vesicle membrane retrieval and synapse development. J. Cell Biol. *178*, 309–322.

Kononenko, N.L., Puchkov, D., Classen, G.A., Walter, A.M., Pechstein, A., Sawade, L., Kaempf, N., Trimbuch, T., Lorenz, D., Rosenmund, C., et al. (2014). Clathrin/AP-2 Mediate Synaptic Vesicle Reformation from Endosome-like Vacuoles but Are Not Essential for Membrane Retrieval at Central Synapses. Neuron *82*, 981–988.

Lee, J.S., Ho, W.-K., and Lee, S.-H. (2012). Actin-dependent rapid recruitment of reluctant synaptic vesicles into a fast-releasing vesicle pool. Proc. Natl. Acad. Sci. U.S.A. *109*, E765-774.

Madania, A., Dumoulin, P., Grava, S., Kitamoto, H., Schärer-Brodbeck, C., Soulard, A., Moreau, V., and Winsor, B. (1999). The Saccharomyces cerevisiae Homologue of Human Wiskott–Aldrich Syndrome Protein Las17p Interacts with the Arp2/3 Complex. MBoC *10*, 3521–3538.

Marie, B., Sweeney, S.T., Poskanzer, K.E., Roos, J., Kelly, R.B., and Davis, G.W. (2004). Dap160/intersectin scaffolds the periactive zone to achieve high-fidelity endocytosis and normal synaptic growth. Neuron *43*, 207–219.

Marra, V., Burden, J.J., Thorpe, J.R., Smith, I.T., Smith, S.L., Häusser, M., Branco, T., and Staras, K. (2012). A Preferentially Segregated Recycling Vesicle Pool of Limited Size Supports Neurotransmission in Native Central Synapses. Neuron *76*, 579–589.

Meinecke, M., Boucrot, E., Camdere, G., Hon, W.-C., Mittal, R., and McMahon, H.T. (2013). Cooperative recruitment of dynamin and BIN/amphiphysin/Rvs (BAR) domain-containing proteins leads to GTP-dependent membrane scission. J. Biol. Chem. *288*, 6651–6661.

Melom, J.E., Akbergenova, Y., Gavornik, J.P., and Littleton, J.T. (2013). Spontaneous and Evoked Release Are Independently Regulated at Individual Active Zones. J Neurosci *33*, 17253–17263.

Merrifield, C.J., Qualmann, B., Kessels, M.M., and Almers, W. (2004). Neural Wiskott Aldrich Syndrome Protein (N-WASP) and the Arp2/3 complex are recruited to sites of clathrin-mediated endocytosis in cultured fibroblasts. Eur. J. Cell Biol. *83*, 13–18.

Morales, M., Colicos, M.A., and Goda, Y. (2000). Actin-Dependent Regulation of Neurotransmitter Release at Central Synapses. Neuron *27*, 539–550.

Moseley, J.B., Maiti, S., and Goode, B.L. (2006). Formin proteins: purification and measurement of effects on actin assembly. Meth. Enzymol. *406*, 215–234.

Mueller, V.J., Wienisch, M., Nehring, R.B., and Klingauf, J. (2004). Monitoring clathrin-mediated endocytosis during synaptic activity. J. Neurosci. *24*, 2004–2012.

Ni, J.-Q., Markstein, M., Binari, R., Pfeiffer, B., Liu, L.-P., Villalta, C., Booker, M., Perkins, L., and Perrimon, N. (2008). Vector and parameters for targeted transgenic RNA interference in *Drosophila* melanogaster. Nat. Methods *5*, 49–51.

Nunes, P., Haines, N., Kuppuswamy, V., Fleet, D.J., and Stewart, B.A. (2006). Synaptic Vesicle Mobility and Presynaptic F-Actin Are Disrupted in a N-ethylmaleimide–sensitive Factor Allele of *Drosophila*. MBoC *17*, 4709–4719.

O'Connor-Giles, K.M., Ho, L.L., and Ganetzky, B. (2008). Nervous Wreck Interacts with Thickveins and the Endocytic Machinery to Attenuate Retrograde BMP Signaling during Synaptic Growth. Neuron *58*, 507–518.

Okamoto, M., Schoch, S., and Südhof, T.C. (1999). EHSH1/intersectin, a protein that contains EH and SH3 domains and binds to dynamin and SNAP-25. A protein connection between exocytosis and endocytosis? J. Biol. Chem. *274*, 18446–18454.

Owe, S.G., Jensen, V., Evergren, E., Ruiz, A., Shupliakov, O., Kullmann, D.M., Storm-Mathisen, J., Walaas, S.I., Hvalby, Ø., and Bergersen, L.H. (2009). Synapsin- and Actin-Dependent Frequency Enhancement in Mouse Hippocampal Mossy Fiber Synapses. Cereb Cortex *19*, 511–523.

Pawson, C., Eaton, B.A., and Davis, G.W. (2008). Formin-Dependent Synaptic Growth: Evidence That Dlar Signals via Diaphanous to Modulate Synaptic Actin and Dynamic Pioneer Microtubules. J. Neurosci. *28*, 11111–11123.

Pechstein, A., Bacetic, J., Vahedi-Faridi, A., Gromova, K., Sundborger, A., Tomlin, N., Krainer, G., Vorontsova, O., Schäfer, J.G., Owe, S.G., et al. (2010). Regulation of synaptic vesicle recycling by

complex formation between intersectin 1 and the clathrin adaptor complex AP2. Proc. Natl. Acad. Sci. U.S.A. *107*, 4206–4211.

Pechstein, A., Gerth, F., Milosevic, I., Jäpel, M., Eichhorn-Grünig, M., Vorontsova, O., Bacetic, J., Maritzen, T., Shupliakov, O., Freund, C., et al. (2015). Vesicle uncoating regulated by SH3-SH3 domain-mediated complex formation between endophilin and intersectin at synapses. EMBO Rep. *16*, 232–239.

Pelassa, I., Zhao, C., Pasche, M., Odermatt, B., and Lagnado, L. (2014). Synaptic vesicles are "primed" for fast clathrin-mediated endocytosis at the ribbon synapse. Front Mol Neurosci *7*, 91–91.

Peng, A., Rotman, Z., Deng, P.-Y., and Klyachko, V.A. (2012). Differential Motion Dynamics of Synaptic Vesicles Undergoing Spontaneous and Activity-Evoked Endocytosis. Neuron *73*, 1108–1115.

Piccioli, Z.D., and Littleton, J.T. (2014). Retrograde BMP Signaling Modulates Rapid Activity-Dependent Synaptic Growth via Presynaptic LIM Kinase Regulation of Cofilin. J. Neurosci. *34*, 4371–4381.

Praefcke, G.J., Ford, M.G., Schmid, E.M., Olesen, L.E., Gallop, J.L., Peak-Chew, S.-Y., Vallis, Y., Babu, M.M., Mills, I.G., and McMahon, H.T. (2004). Evolving nature of the AP2 α-appendage hub during clathrin-coated vesicle endocytosis. The EMBO Journal *23*, 4371–4383.

Pucharcos, C., Estivill, X., and de la Luna, S. (2000). Intersectin 2, a new multimodular protein involved in clathrin-mediated endocytosis11The sequence data reported in this paper have been submitted to GenBank and have been assigned the accession numbers AF182198 and AF182199. FEBS Letters *478*, 43–51.

Ramachandran, P., and Budnik, V. (2010). FM1-43 Labeling of *Drosophila* Larval Neuromuscular Junctions. Cold Spring Harb Protoc *2010*, pdb.prot5471.

Rao, Y., Ma, Q., Vahedi-Faridi, A., Sundborger, A., Pechstein, A., Puchkov, D., Luo, L., Shupliakov, O., Saenger, W., and Haucke, V. (2010). Molecular basis for SH3 domain regulation of F-BAR-mediated membrane deformation. Proc. Natl. Acad. Sci. U.S.A. *107*, 8213–8218.

Rodal, A.A., Motola-Barnes, R.N., and Littleton, J.T. (2008). Nervous wreck and Cdc42 cooperate to regulate endocytic actin assembly during synaptic growth. J. Neurosci. *28*, 8316–8325.

Rodal, A.A., Blunk, A.D., Akbergenova, Y., Jorquera, R.A., Buhl, L.K., and Littleton, J.T. (2011). A presynaptic endosomal trafficking pathway controls synaptic growth signaling. J. Cell Biol. *193*, 201–217.

Roos, J., and Kelly, R.B. (1998). Dap160, a neural-specific Eps15 homology and multiple SH3 domain-containing protein that interacts with *Drosophila* dynamin. J. Biol. Chem. *273*, 19108–19119.

Sakaba, T., and Neher, E. (2003). Involvement of Actin Polymerization in Vesicle Recruitment at the Calyx of Held Synapse. J. Neurosci. *23*, 837–846.

Sankaranarayanan, S., Atluri, P.P., and Ryan, T.A. (2003). Actin has a molecular scaffolding, not propulsive, role in presynaptic function. Nat. Neurosci. *6*, 127–135.

Schmid, E.M., Ford, M.G.J., Burtey, A., Praefcke, G.J.K., Peak-Chew, S.-Y., Mills, I.G., Benmerah, A., and McMahon, H.T. (2006). Role of the AP2 β-Appendage Hub in Recruiting Partners for Clathrin-Coated Vesicle Assembly. PLOS Biology *4*, e262.

Sengar, A.S., Wang, W., Bishay, J., Cohen, S., and Egan, S.E. (1999). The EH and SH3 domain Ese proteins regulate endocytosis by linking to dynamin and Eps15. EMBO J. *18*, 1159–1171.

Sone, M., Suzuki, E., Hoshino, M., Hou, D., Kuromi, H., Fukata, M., Kuroda, S., Kaibuchi, K., Nabeshima, Y., and Hama, C. (2000). Synaptic development is controlled in the periactive zones of *Drosophila* synapses. Development *127*, 4157–4168.

Soykan, T., Kaempf, N., Sakaba, T., Vollweiter, D., Goerdeler, F., Puchkov, D., Kononenko, N.L., and Haucke, V. (2017). Synaptic Vesicle Endocytosis Occurs on Multiple Timescales and Is Mediated by Formin-Dependent Actin Assembly. Neuron *93*, 854-866.e4.

Spudich, J.A., and Watt, S. (1971). The regulation of rabbit skeletal muscle contraction. I. Biochemical studies of the interaction of the tropomyosin-troponin complex with actin and the proteolytic fragments of myosin. J. Biol. Chem. *246*, 4866–4871.

Stanishneva-Konovalova, T.B., Kelley, C.F., Eskin, T.L., Messelaar, E.M., Wasserman, S.A., Sokolova, O.S., and Rodal, A.A. (2016). Coordinated autoinhibition of F-BAR domain membrane binding and WASp activation by Nervous Wreck. Proc. Natl. Acad. Sci. U.S.A. *113*, E5552-5561.

Stewart, B.A., Atwood, H.L., Renger, J.J., Wang, J., and Wu, C.F. (1994). Improved stability of *Drosophila* larval neuromuscular preparations in haemolymph-like physiological solutions. J. Comp. Physiol. A *175*, 179–191.

Sun, Y., Leong, N.T., Jiang, T., Tangara, A., Darzacq, X., and Drubin, D.G. Switch-like Arp2/3 activation upon WASP and WIP recruitment to an apparent threshold level by multivalent linker proteins in vivo. eLife *6*.

Teckchandani, A., Mulkearns, E.E., Randolph, T.W., Toida, N., and Cooper, J.A. (2012). The clathrin adaptor Dab2 recruits EH domain scaffold proteins to regulate integrin β1 endocytosis. Mol. Biol. Cell *23*, 2905–2916.

Ukken, F.P., Bruckner, J.J., Weir, K.L., Hope, S.J., Sison, S.L., Birschbach, R.M., Hicks, L., Taylor, K.L., Dent, E.W., Gonsalvez, G.B., et al. (2016). BAR-SH3 sorting nexins are conserved interacting proteins of Nervous wreck that organize synapses and promote neurotransmission. J. Cell. Sci. *129*, 166–177.

Verstreken, P., Ohyama, T., and Bellen, H.J. (2008). FM 1-43 labeling of synaptic vesicle pools at the *Drosophila* neuromuscular junction. Methods Mol. Biol. *440*, 349–369.

Wagh, D., Terry-Lorenzo, R., Waites, C.L., Leal-Ortiz, S.A., Maas, C., Reimer, R.J., and Garner, C.C. (2015). Piccolo Directs Activity Dependent F-Actin Assembly from Presynaptic Active Zones via Daam1. PLOS ONE *10*, e0120093.

Waites, C.L., Leal-Ortiz, S.A., Andlauer, T.F.M., Sigrist, S.J., and Garner, C.C. (2011). Piccolo Regulates the Dynamic Assembly of Presynaptic F-Actin. J. Neurosci. *31*, 14250–14263.

Wang, D., Zhang, L., Zhao, G., Wahlström, G., Heino, T.I., Chen, J., and Zhang, Y.Q. (2010). *Drosophila* twinfilin is required for cell migration and synaptic endocytosis. J Cell Sci *123*, 1546–1556.

Wang, J.-W., Brent, J.R., Tomlinson, A., Shneider, N.A., and McCabe, B.D. (2011). The ALS-associated proteins FUS and TDP-43 function together to affect *Drosophila* locomotion and life span. J. Clin. Invest. *121*, 4118–4126.

Wang, X., Kibschull, M., Laue, M.M., Lichte, B., Petrasch-Parwez, E., and Kilimann, M.W. (1999). Aczonin, a 550-Kd Putative Scaffolding Protein of Presynaptic Active Zones, Shares Homology Regions with Rim and Bassoon and Binds Profilin. J Cell Biol *147*, 151–162.

Watanabe, S., Rost, B.R., Camacho-Pérez, M., Davis, M.W., Söhl-Kielczynski, B., Rosenmund, C., and Jorgensen, E.M. (2013). Ultrafast endocytosis at mouse hippocampal synapses. Nature *504*, 242–247.

Wienisch, M., and Klingauf, J. (2006). Vesicular proteins exocytosed and subsequently retrieved by compensatory endocytosis are nonidentical. Nat. Neurosci. *9*, 1019–1027.

Wilhelm, B.G., Mandad, S., Truckenbrodt, S., Kröhnert, K., Schäfer, C., Rammner, B., Koo, S.J., Claßen, G.A., Krauss, M., Haucke, V., et al. (2014). Composition of isolated synaptic boutons reveals the amounts of vesicle trafficking proteins. Science *344*, 1023–1028.

Winther, Å.M.E., Jiao, W., Vorontsova, O., Rees, K.A., Koh, T.-W., Sopova, E., Schulze, K.L., Bellen, H.J., and Shupliakov, O. (2013). The dynamin-binding domains of Dap160/intersectin affect bulk membrane retrieval in synapses. J. Cell. Sci. *126*, 1021–1031.

Winther, Å.M.E., Vorontsova, O., Rees, K.A., Näreoja, T., Sopova, E., Jiao, W., and Shupliakov, O. (2015). An Endocytic Scaffolding Protein together with Synapsin Regulates Synaptic Vesicle Clustering in the *Drosophila* Neuromuscular Junction. J. Neurosci. *35*, 14756–14770.

Wolf, M., Zimmermann, A.-M., Görlich, A., Gurniak, C.B., Sassoè-Pognetto, M., Friauf, E., Witke, W., and Rust, M.B. (2015). ADF/Cofilin Controls Synaptic Actin Dynamics and Regulates Synaptic Vesicle Mobilization and Exocytosis. Cereb. Cortex *25*, 2863–2875.

Wu, X.-S., Lee, S.H., Sheng, J., Zhang, Z., Zhao, W.-D., Wang, D., Jin, Y., Charnay, P., Ervasti, J.M., and Wu, L.-G. (2016). Actin Is Crucial for All Kinetically Distinguishable Forms of Endocytosis at Synapses. Neuron *92*, 1020–1035.

Xiao, G.-Y., Mohanakrishnan, A., and Schmid, S.L. (2018). Role for ERK1/2-dependent activation of FCHSD2 in cancer cell-selective regulation of clathrin-mediated endocytosis. PNAS *115*, E9570–E9579.